# Mobile impurity approach to the optical conductivity in the Hubbard chain

Thomas Veness and Fabian H. L. Essler
*The Rudolf Peierls Centre for Theoretical Physics, University of Oxford, Oxford OX1 3NP, UK*

We consider the optical conductivity in the one dimensional Hubbard model in the metallic phase close to half filling. In this regime most of the spectral weight is located at frequencies above an energy scale $E_{\rm opt}$ that tends towards the optical gap in the Mott insulating phase for vanishing doping. Using the Bethe Ansatz we relate $E_{\rm opt}$ to thresholds of particular kinds of excitations in the Hubbard model. We then employ a mobile impurity models to analyze the optical conductivity for frequencies slightly above these thresholds. This entails generalizing mobile impurity models to excited states that are not highest weight with regards to the SU(2) symmetries of the Hubbard chain, and that occur at a maximum of the impurity dispersion.

## I. INTRODUCTION

Electron-electron interactions play a crucial rôle in determining the physical response to external probes of various quasi-one-dimensional materials e.g. organic semiconductors[1]. In order to successfully describe the mechanisms and excitations responsible for distinct physical phenomena, it is imperative to have a microscopic model capturing the essence of the physics involved; providing a framework within which realistic physical systems may be interpreted. The one-dimensional Hubbard model[2] offers an excellent theoretical laboratory in which a comprehensive microscopic understanding of the origin of various behaviours can be developed. The Hamiltonian for the Hubbard model is given by

$$\begin{aligned} H = &-t\sum_{i,\sigma} c^\dagger_{i+1,\sigma}c_{i,\sigma} + c^\dagger_{i,\sigma}c_{i+1,\sigma} + U\sum_i n_{i,\uparrow}n_{i,\downarrow} \\ &- \mu\sum_i (n_{i,\uparrow}+n_{i,\downarrow}) - B\sum_i (n_{i,\uparrow}-n_{i,\downarrow}). \end{aligned} \tag{1}$$

Here, $c_{j,\sigma}$ annihilates a fermion with spin $\sigma = \uparrow,\downarrow$ at site $j$, $n_{j,\sigma} = c^\dagger_{j,\sigma}c_{j,\sigma}$ is the number operator, $t$ is the hopping parameter, $\mu$ is the chemical potential, $B$ is the magnetic field, and $U \geq 0$ is the strength of the on-site repulsion.

The low-energy degrees of freedom in the metallic phase of the Hubbard chain are described[2–4] by a (perturbed) spin-charge separated Luttinger liquid[5–8], with Hamiltonian

$$H = \sum_{\alpha=c,s} \frac{v_\alpha}{16\pi}\int {\rm d}x\, \left[\frac{1}{K_\alpha}\left(\frac{\partial\Phi_\alpha}{\partial x}\right)^2 + K_\alpha\left(\frac{\partial\Theta_\alpha}{\partial x}\right)^2\right] + \text{irrelevant operators.} \tag{2}$$

The parameters $K_\alpha$, $v_\alpha$ can be calculated for the Hubbard model by solving a system of linear integral equations (see Appendix A). The Bose fields $\Phi_\alpha(x)$ and dual fields $\Theta_\alpha(x)$ obey the commutation relation

$$[\Phi_\alpha(x),\Theta_\beta(y)] = 4\pi i\delta_{\alpha\beta}{\rm sgn}(x-y). \tag{3}$$

The spectrum of low-lying excitations relative to the ground state for a large but finite system of length $L$ in zero magnetic field is given by[2–4]

$$\Delta E = \frac{2\pi v_c}{L}\left[\frac{(\Delta N_c)^2}{8K_c} + 2K_c\left(D_c+\frac{D_s}{2}\right)^2 + N_c^+ + N_c^-\right] + \frac{2\pi v_s}{L}\left[\frac{\left(\Delta N_s - \frac{\Delta N_c}{2}\right)^2}{2} + \frac{D_s^2}{2} + N_s^+ + N_s^-\right], \tag{4}$$

where $\Delta N_\alpha$, $D_\alpha$ and $N_\alpha^\pm$ are integers or half-odd integers subject to the "selection rules"

$$N_\alpha^\pm \in \mathbb{N}_0, \qquad \Delta N_\alpha \in \mathbb{Z}, \qquad D_c = \frac{\Delta N_c + \Delta N_s}{2} \bmod 1, \qquad D_s = \frac{\Delta N_c}{2} \bmod 1. \tag{5}$$

At low energies, correlation functions can be calculated from (2) and generically exhibit singularities at the thresholds of the allowed collective spin and charge degrees of freedom, with power-law exponents given in terms of the quantities $\Delta N_\alpha$, $D_\alpha$ and $N_\alpha^\pm$. However, when working at a finite energy scale RG irrelevant terms have a non-zero coupling and may (and in fact generically do) significantly alter the predictions of the unperturbed Luttinger-liquid[9–35]. Over the last decade or so a fairly general method for taking into account the effects of certain irrelevant operators in

the vicinities of kinematic thresholds has been developed, which is reviewed in Refs. 36 and 38. The case of spin-charge separated Luttinger liquids has very recently been revisited[35] in order to make it explicitly compatible with exactly known properties of the Hubbard model. The essence of this approach is that, when considering a response function, there are thresholds in the $(k,\omega)$-plane that correspond to particular excitations. In integrable models, these excitations hold privileged positions: they are stable (i.e. have infinite lifetimes) and can be identified in terms of the exact solution. If the kinematics near the threshold are described by a case in which small number of high-energy excitations carry most of the energy (in the precise sense of up to corrections of $\mathcal{O}(L^{-1})$) then the problem becomes analogous to that of the X-ray edge singularity problem for a mobile impurity[39].

In this work we employ mobile impurity methods to study the optical conductivity

$$\sigma_1(\omega) = -\frac{\mathrm{Im}\,\chi^J(\omega)}{\omega}, \qquad \chi^J(\omega) = -ie^2\int_0^\infty dt\; e^{i\omega t}\sum_{l=-L/2}^{L/2-1}\langle GS|[J_l(t),J_0(0)]|GS\rangle, \tag{6}$$

where $J_j$ is the density of the current operator

$$J_j = -it\sum_\sigma\left[c^\dagger_{j,\sigma}c_{j+1,\sigma} - c^\dagger_{j+1,\sigma}c_{j,\sigma}\right]. \tag{7}$$

In the Mott insulating phase of the Hubbard model the optical conductivity has been previously determined[40–44]: $\sigma_1(\omega)$ vanishes inside the optical gap $2\Delta$, where $\Delta$ is the Mott gap. At frequencies $\omega > 2\Delta$ there is a sudden power-law onset $\sigma_1(\omega)\sim\sqrt{\omega-2\Delta}$. Away from half-filling, the system is a metal and therefore has a finite conductivity for all $\omega$, specifically acquiring a Drude peak[45,46] at $\omega = 0$. The low-frequency behaviour has been previously studied[47–49] in the framework of Luttinger liquid theory, predicting $\omega^3$ behaviour for $0<\omega\ll t$. Close to half-filling one expects most of the spectral weight in $\sigma_1(\omega)$ to be located above an energy scale $E_{\rm opt}$ that tends to $2\Delta$ as we approach half-filling. The scale $E_{\rm opt}$ has been previously correctly identified in Ref. 50. In the same work it was conjectured that the optical conductivity increases in a power-law fashion above $E_{\rm opt}$

$$\sigma_1(\omega)\sim(\omega-E_{\rm opt})^\zeta\;\Theta(\omega-E_{\rm opt})\;. \tag{8}$$

As we will see in the following, the mobile impurity approach leads to different results.

The outline of this paper is as follows. In Sec. II, we consider the spectral representation of the optical conductivity and identify the quantum numbers of the states contributing non-zero spectral weight. In Sec. III we review the Bethe Ansatz description of the ground state and construct the excited states considered in Sec. II, specifically identifying the thresholds of these continua. In Sec. IV we calculate the threshold/edge behaviour for the associated excitations via the mobile impurity approach, fixing the coupling constants using the Bethe Ansatz to determine the finite-size corrections to the energy in the presence of the high-energy excitation.

## II. SPECTRAL REPRESENTATION OF THE CURRENT-CURRENT CORRELATOR

In considering the optical conductivity as defined in (6), the basic quantity of interest is

$$\langle GS|J_{j+\ell}(t)J_j(0)|GS\rangle = \sum_n\langle GS|J_{j+\ell}|n\rangle\langle n|J_j|GS\rangle e^{-i(E_n-E_{GS})t}, \tag{9}$$

where $\{|n\rangle\}$ constitute a complete set of energy eigenstates. To understand threshold behaviours, we wish to identify the states contributing to this sum. A crucial insight to this end are global continuous symmetries and their relation to the energy eigenstates provided by the exact Bethe Ansatz solution[51–55]. In the case of zero magnetic field and chemical potential, the Hubbard model possesses two independent SU(2) symmetries[2,56,57]:

$$\begin{aligned}
S^z &= \frac{1}{2}\sum_{i=1}^L(c^\dagger_{i,\uparrow}c_{i,\uparrow}-c^\dagger_{i,\downarrow}c_{i,\downarrow}), & S^+ &= \sum_{i=1}^L c^\dagger_{i,\uparrow}c_{i,\downarrow}, & S^- &= \sum_{i=1}^L c^\dagger_{i,\downarrow}c_{i,\uparrow}\;,\\
\eta^z &= \frac{1}{2}\sum_{i=1}^L(c^\dagger_{i,\uparrow}c_{i,\uparrow}+c^\dagger_{i,\downarrow}c_{i,\downarrow}-1), & \eta^+ &= \sum_{i=1}^L(-1)^i c^\dagger_{i,\downarrow}c^\dagger_{i,\uparrow}, & \eta^- &= \sum_{i=1}^L(-1)^i c_{i,\uparrow}c_{i,\downarrow}.
\end{aligned} \tag{10}$$

The $S^\alpha$ generate the well known spin rotational SU(2) symmetry, while the $\eta^\alpha$ are known as $\eta$-pairing generators. The Bethe Ansatz provides us with the *lowest weight states*[51], which we denote by $|LWS;\mathbf{m}\rangle$. Here $\mathbf{m}$ is a multi-index

which labels all distinct regular Bethe Ansatz states in the sense of Ref. 51. The states are lowest-weight with respect to the two SU(2) algebras in the sense that

$$\eta^-|LWS;\mathbf{m}\rangle = 0 = S^+|LWS;\mathbf{m}\rangle \ . \tag{11}$$

Each state $|LWS;\mathbf{m}\rangle$ is defined on a system of length $L$ and has a well-defined number of electrons $N$ and $z$-component of spin $S_z$. A complete basis of states is given by $\left\{(\eta^+)^k(S^-)^l|LWS;\mathbf{m}\rangle \mid k=0,\ldots,L-N;\ l=0,\ldots,2S^z\right\}$. For the repulsive Hubbard model below half-filling, the ground state in zero magnetic field and finite chemical potential is a spin singlet and a lowest-weight $\eta$-pairing state i.e.

$$S^-|GS\rangle = S^+|GS\rangle = \eta^-|GS\rangle = 0. \tag{12}$$

Using the algebra defined in (10) it is readily verified that $[\eta^-,[\eta^-,J_j]]=0$ and therefore for integer $m\geq 0$

$$\langle LWS;\mathbf{n}|(\eta^-)^{m+1}J_j|GS\rangle = \langle LWS;\mathbf{n}|(\eta^-)^m[\eta^-,J_j]|GS\rangle = \delta_{m,0}\langle LWS;\mathbf{n}|[\eta^-,J_j]|GS\rangle. \tag{13}$$

This shows that the only states that may have a non-zero overlap with $J_j|GS\rangle$ are lowest weight states $|LWS;\mathbf{m}\rangle$ or $\eta$-pairing descendant states of the form $\eta^+|LWS;\mathbf{m}\rangle$, which implies the expansion

$$J_j|GS\rangle = \sum_{\mathbf{m}} \left(a_{\mathbf{m}}|LWS;\mathbf{m}\rangle + b_{\mathbf{m}}\eta^+|LWS;\mathbf{m}\rangle\right), \tag{14}$$

where $a_{\mathbf{m}}$, $b_{\mathbf{m}}$ are complex coefficients. Substituting this into (9) provides further constraints on the subset of energy eigenstates that may make non-vanishing contributions to the correlator. The subset consists of

1. Lowest-weight states with $N_{GS}$ electrons with $\mathbf{S}^2=S^z=0$;
2. States of the form $\eta^+|LWS;\mathbf{m}\rangle$, with $|LWS;\mathbf{m}\rangle$ having $N_{GS}-2$ electrons and $\mathbf{S}^2=S^z=0$.

Using that $[H,\eta^+]=-2\mu\eta^+$ we can thus express the current-current correlator in the form

$$\begin{aligned} C_{\mathrm{JJ}}(\ell,t) &= \langle GS|J_{j+\ell}(t)J_j(0)|GS\rangle \\ &= \sum_{\mathbf{m}}\langle GS|J_{j+\ell}|LWS;\mathbf{m}\rangle\langle LWS;\mathbf{m}|J_j|GS\rangle e^{-i(E_{\mathbf{m}}-E_{GS})t} \\ &+ \sum_{\mathbf{m}}\frac{1}{2\eta^z_{\mathbf{m}}}\langle GS|J_{j+\ell}\eta^+|LWS;\mathbf{m}\rangle\langle LWS;\mathbf{m}|\eta^-J_j|GS\rangle e^{-i(E_{\mathbf{m}}-E_{GS}-2\mu)t}. \end{aligned} \tag{15}$$

The factor of $(2\eta^z_{\mathbf{m}})^{-1}$ arises from the normalization of the state $\eta^+|LWS,\mathbf{m}\rangle$. We note that $\mu<0$ and hence $-2\mu$ is a positive energy shift. It is not obvious how to understand the second term in the framework of a mobile impurity model. However, using the lowest-weight property $\eta^-|GS\rangle=0$, we can rewrite (15) in the form

$$\begin{aligned} C_{\mathrm{JJ}}(\ell,t) &= \sum_{\mathbf{m}}\langle GS|J_{j+\ell}|LWS;\mathbf{m}\rangle\langle LWS;\mathbf{m}|J_j|GS\rangle e^{-i(E_{\mathbf{m}}-E_{GS})t} \\ &+ \sum_{\mathbf{m}}\frac{1}{2\eta^z_{\mathbf{m}}}\langle GS|[J_{j+\ell},\eta^+]|LWS;\mathbf{m}\rangle\langle LWS;\mathbf{m}|[\eta^-,J_j]|GS\rangle e^{-i(E_{\mathbf{m}}-E_{GS}-2\mu)t}. \end{aligned} \tag{16}$$

The main advantage of the representation (16) is that it only involves regular Bethe Ansatz states, which can be constructed by standard methods. As we concern ourselves only with the threshold behaviours of the optical conductivity, we need only focus on the lower edges of the various excitation continua. As a consequence of kinematic constraints and matrix-element effects, processes with a small number of excitations above the ground state give the dominant contributions to response functions. Defining

$$\mathcal{O}_j = [\eta^-,J_j] = 2it(-1)^j\left(c_{j,\downarrow}c_{j+1,\uparrow}+c_{j+1,\downarrow}c_{j,\uparrow}\right), \tag{17}$$

we can recast (16) in the form

$$\begin{aligned} C_{\mathrm{JJ}}(\ell,t) &= \sum_{\mathbf{m}}|\langle GS|J_j|LWS;\mathbf{m}\rangle|^2 e^{-i(E_{\mathbf{m}}-E_{GS})t+iP_{\mathbf{m}}\ell} \\ &+ \sum_{\mathbf{m}}\frac{1}{2\eta^z_{\mathbf{m}}}|\langle GS|\mathcal{O}_j^\dagger|LWS;\mathbf{m}\rangle|^2 e^{-i(E_{\mathbf{m}}-E_{GS}-2\mu)t+i(P_{\mathbf{m}}-\pi)\ell} \equiv C^{(1)}_{\mathrm{JJ}}(\ell,t)+C^{(2)}_{\mathrm{JJ}}(\ell,t). \end{aligned} \tag{18}$$

Here the additional contribution to the momentum arises because acting with $\eta^+$ shifts the momentum by $\pi$. If the ground state contains $N$ fermions, the contribution $C^{(2)}_{\rm JJ}(\ell,t)$ is proportional to $1/(L-N+2)$, and can therefore be dropped in the thermodynamic limit away from half filling. However, as we are interested in densities close to one fermion per site it is useful to retain it in view of potential comparisons to numerical results for finite-size systems. The optical conductivity can then be written as

$$\sigma_1(\omega)=\frac{e^2}{2\omega}\left[\sum_{a=1}^{2}\sum_{\ell}\int_{-\infty}^{\infty}dt\; e^{i\omega t}\; C^{(a)}_{\rm JJ}(\ell,t)-\{\omega\to-\omega\}\right]\equiv\sum_{a=1}^{2}\sigma_1^{(a)}(\omega). \tag{19}$$

## III. BETHE ANSATZ FOR THE HUBBARD MODEL

To gain further insight into the representation (18) we now construct the ground state and low-lying excitations above it. We first calculate the energy of such excitations in the thermodynamic limit. This will allow us to identify, on kinematic grounds, which states within the manifold identified earlier are important with respect to the threshold behaviours we aim to describe. We therefore recapitulate some results from Ref. 2 to allow a self-contained discussion.

For large system sizes, the eigenstates of the repulsive Hubbard model can be expressed in terms of solutions of the Takahashi equations, expressed in terms of so-called *counting functions*. In the case of $N$ electrons, $M$ of which are spin-down, these are defined by

$$z_c(k_j)=k_j+\frac{1}{L}\sum_{n=1}^{\infty}\sum_{\alpha=1}^{M_n}\theta\left(\frac{\sin k_j-\Lambda^n_\alpha}{nu}\right)+\frac{1}{L}\sum_{n=1}^{\infty}\sum_{\alpha=1}^{M'_n}\theta\left(\frac{\sin k_j-{\Lambda'}^n_\alpha}{nu}\right),\qquad j=1,\ldots,N-2M', \tag{20}$$

$$z_n(\Lambda^n_\alpha)=\frac{1}{L}\sum_{j=1}^{N-2M'}\theta\left(\frac{\Lambda^n_\alpha-\sin k_j}{nu}\right)-\frac{1}{L}\sum_{m=1}^{\infty}\sum_{\beta=1}^{M_m}\Theta_{nm}\left(\frac{\Lambda^n_\alpha-\Lambda^m_\beta}{u}\right),\qquad \alpha=1,\ldots,M_n, \tag{21}$$

$$\begin{aligned}z'_n({\Lambda'}^n_\alpha)=&-\frac{1}{L}\sum_{j=1}^{N-2M'}\theta\left(\frac{{\Lambda'}^n_\alpha-\sin k_j}{nu}\right)-\frac{1}{L}\sum_{m=1}^{\infty}\sum_{\beta=1}^{M'_m}\Theta_{nm}\left(\frac{{\Lambda'}^n_\alpha-{\Lambda'}^m_\beta}{u}\right)\\&+2\mathrm{Re}[\arcsin({\Lambda'}^n_\alpha+niu)],\qquad \alpha=1,\ldots,M'_n,\end{aligned} \tag{22}$$

where $\theta(x)=2\arctan(x)$, $u=U/4t$,

$$\Theta_{nm}(x)=\begin{cases}\theta\left(\frac{x}{|n-m|}\right)+2\theta\left(\frac{x}{|n-m|+2}\right)+\cdots+2\theta\left(\frac{x}{n+m-2}\right)+\theta\left(\frac{x}{n+m}\right), & n\neq m\\ 2\theta\left(\frac{x}{2}\right)+2\theta\left(\frac{x}{4}\right)+\cdots+2\theta\left(\frac{x}{2n-2}\right)+\theta\left(\frac{x}{2n}\right), & n=m\end{cases}, \tag{23}$$

and

$$M=\sum_{n=1}^{\infty}n(M_n+M'_n),\qquad M'=\sum_{n=1}^{\infty}nM'_n. \tag{24}$$

Takahashi's equations are

$$z_c(k_j)=\frac{2\pi I_j}{L},\qquad z_n(\Lambda^n_\alpha)=\frac{2\pi J^n_\alpha}{L},\qquad z'_n({\Lambda'}^n_\alpha)=\frac{2\pi {J'}^n_\alpha}{L}. \tag{25}$$

Here the sets $\{I_j\}$, $\{J^n_\alpha\}$, $\{{J'}^n_\alpha\}$ consist of integers or half-odd integers depending on the particular state under consideration, obeying the "selection rules"

$$\begin{aligned}I_j&\in\begin{cases}\mathbb{Z}+\frac{1}{2} & \text{if } \sum_m(M_m+M'_m) \text{ odd}\\ \mathbb{Z} & \text{if } \sum_m(M_m+M'_m) \text{ even}\end{cases}, && -\frac{L}{2}<I_j\leq\frac{L}{2},\\ J^n_\alpha&\in\begin{cases}\mathbb{Z} & \text{if } N-M_n \text{ odd}\\ \mathbb{Z}+\frac{1}{2} & \text{if } N-M_n \text{ even}\end{cases}, && |J^n_\alpha|\leq\frac{1}{2}(N-2M'-\sum_{m=1}^{\infty}t_{nm}M_m-1),\\ {J'}^n_\alpha&\in\begin{cases}\mathbb{Z} & \text{if } L-N+M'_n \text{ odd}\\ \mathbb{Z}+\frac{1}{2} & \text{if } L-N+M'_n \text{ even}\end{cases}, && |{J'}^n_\alpha|\leq\frac{1}{2}\left(L-N+2M'-\sum_{m=1}^{\infty}t_{nm}M'_m-1\right),\end{aligned} \tag{26}$$

where $t_{nm} = 2\min(m,n) - \delta_{mn}$. The energy and momentum, measured in units of $t$, of an eigenstate characterised by the set of roots $\{k_j, \Lambda^n_\alpha, \Lambda'^m_\beta\}$ are given by

$$E = -\sum_{j=1}^{N-2M'} (2\cos k_j + \mu + 2u + B) + 2BM + 4\sum_{n=1}^{\infty}\sum_{\beta=1}^{M'_n} \mathrm{Re}\sqrt{1-(\Lambda'^n_\beta + niu)^2} + Lu, \tag{27}$$

$$P = \left[\sum_{j=1}^{N-2M'} k_j - \sum_{n=1}^{\infty}\sum_{\beta=1}^{M'_n} \left(2\,\mathrm{Re}\arcsin\left(\Lambda'^n_\beta + niu\right) - (n+1)\pi\right)\right] \bmod 2\pi. \tag{28}$$

The monotonicity of the counting functions ensures that specifying a set of integers/half-odd integers in accordance with the "selection rules" uniquely determines a solution of the Takahashi equations.

### A. Ground state

We consider the case where $L$ is even, the total number of electrons $N_{GS}$ is even and the number of down spins $M_{GS}$ is odd. The ground state is then obtained by choosing the set $\{I_j, J^n_\alpha, J'^m_\beta\}$ to be[2]

$$I_j = -\frac{N_{GS}}{2} - \frac{1}{2} + j, \qquad j = 1, \ldots, N_{GS}, \tag{29}$$

$$J^1_\alpha = -\frac{M_{GS}}{2} - \frac{1}{2} + \alpha, \qquad \alpha = 1, \ldots, M_{GS}. \tag{30}$$

This configuration is shown for the example $L = 16$, $N_{GS} = 2M_{GS} = 10$ in Fig. 1. We denote the ground state, in the previously established notation, by

$$|GS\rangle = |LWS; \{I_j\}, \{J^1_\alpha\}\rangle. \tag{31}$$

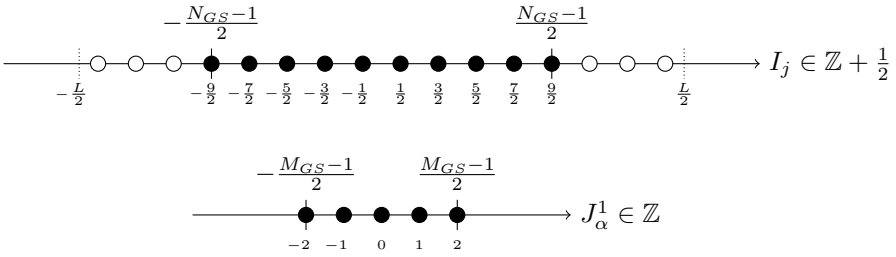


Figure 1: Configuration of the integers for the ground state, explicit numbers given are for $L = 16$, $N_{GS} = 10$, $M_{GS} = 5$

#### 1. *Thermodynamic limit*

On taking the thermodynamic limit at fixed density $n_{GS}$ and magnetisation $m_{GS}$ the roots become dense and we can describe the ground state in terms of root densities $\rho_{c,0}$, $\rho_{s,0}$, which satisfy linear integral equations[2]

$$\rho_{c,0}(k) = \frac{1}{2\pi} + \cos k \int_{-A}^{A} \mathrm{d}\Lambda\, a_1(\sin k - \Lambda)\rho_{s,0}(\Lambda), \tag{32}$$

$$\rho_{s,0}(\Lambda) = \int_{-Q}^{Q} \mathrm{d}k\, a_1(\Lambda - \sin k)\rho_{c,0}(k) - \int_{-A}^{A} \mathrm{d}\Lambda'\, a_2(\Lambda - \Lambda')\rho_{s,0}(\Lambda'). \tag{33}$$

Here $a_n(x) = \frac{2nu}{2\pi}\frac{1}{(nu)^2+x^2}$ and the integration boundaries $Q$ and $A$ are determined by

$$\int_{-Q}^{Q} \mathrm{d}k\, \rho_{c,0}(k) = n_{GS}, \qquad \int_{-A}^{A} \mathrm{d}\Lambda\, \rho_{s,0}(\Lambda) = \frac{1}{2}\left(n_{GS} - 2m_{GS}\right). \tag{34}$$

The energy density of the system is given to $o(1)$ by[2]

$$e_{GS} = \int_{-Q}^{Q} \frac{\mathrm{d}k}{2\pi}\varepsilon_c(k) + u, \tag{35}$$

where

$$\varepsilon_c(k) = -2\cos k - \mu - 2u - B + \int_{-A}^{A} \mathrm{d}\Lambda\, a_1(\sin k - \Lambda)\varepsilon_s(\Lambda), \tag{36}$$

$$\varepsilon_s(\Lambda) = 2B + \int_{-Q}^{Q} \mathrm{d}k\, \cos k\, a_1(\Lambda - \sin k)\varepsilon_c(k) - \int_{-A}^{A} \mathrm{d}\Lambda'\, a_2(\Lambda - \Lambda')\varepsilon_s(\Lambda'). \tag{37}$$

The dressed energies $\varepsilon_c(k)$ and $\varepsilon_s(\Lambda)$ satisfy $\varepsilon_c(\pm Q) = \varepsilon_s(\pm A) = 0$. The dressed momenta are given by[2]

$$p_c(k) = k + \int_{-A}^{A} \mathrm{d}\Lambda\, \rho_{s,0}(\Lambda)\theta\left(\frac{\sin k - \Lambda}{u}\right), \tag{38}$$

$$p_s(\Lambda) = \int_{-Q}^{Q} \mathrm{d}k\, \rho_{c,0}(k)\theta\left(\frac{\Lambda - \sin k}{u}\right) - \int_{-A}^{A} \mathrm{d}\Lambda'\, \rho_{s,0}(\Lambda')\theta\left(\frac{\Lambda - \Lambda'}{2u}\right). \tag{39}$$

### B. Excitations contributing to $C^{(1)}_{\mathrm{JJ}}(\ell, t)$.

We now turn to excited states that contribute to the spectral representation (18) of $C^{(1)}_{\mathrm{JJ}}(\ell, t)$. These are lowest weight states of the spin and $\eta$-pairing SU(2) algebras with quantum numbers $N = N_{GS}$, $M = M_{GS}$.

#### 1. *"Particle-hole" excitation with $N = N_{GS}$, $M = M_{GS}$.*

Creating a particle-hole excitation in the charge degrees of freedom yields a state with the same charge and spin quantum numbers as the ground state, but with a finite momentum and energy difference. The (half-odd) integers for this type of excitation are given by

$$I_j = \begin{cases} -\frac{N_{GS}+1}{2} + j + \Theta\left(-\frac{N_{GS}+1}{2} + j - I^h\right), & j = 1, \ldots, N_{GS} - 1 \\ I^p, & j = N_{GS} \end{cases}, \tag{40}$$

$$J_\alpha = -\frac{M_{GS}+1}{2} + \alpha, \qquad \alpha = 1, \ldots, M_{GS}, \tag{41}$$

where $\Theta(x) = 1$ for $x \geq 0$ and 0 otherwise. The arrangement for these integers is shown in Fig. 2. This excitation is two-parametric and has an energy and momentum of the form

$$\begin{aligned} E &= e_{GS}L + \varepsilon_c(k^p) - \varepsilon_c(k^h) + o(1), \\ P &= p_c(k^p) - p_c(k^h) + o(1), \end{aligned} \tag{42}$$

where the rapidities are determined by $z_c(k^h) = \frac{2\pi I^h}{L}$, $z_c(k^p) = \frac{2\pi I^p}{L}$. This forms a continuum of excitations above the ground state, shown in Fig. 3.

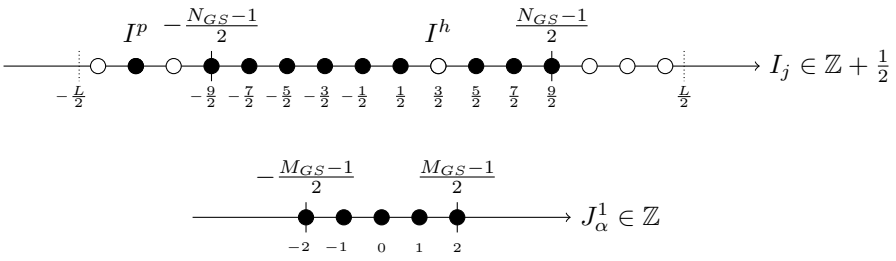


Figure 2: Configuration of the integers for the particle-hole excitation above the ground state, explicit numbers given are for $L = 16$, $N_{GS} = 10$, $M_{GS} = 5$

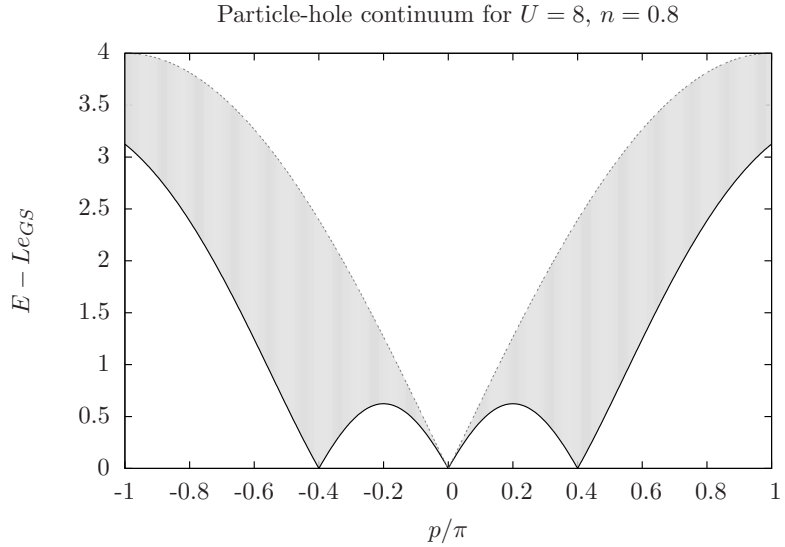


Figure 3: Particle-hole excitation continuum above the ground state

### *2. "k-Λ string" excitation*

We start by considering excitations with $N = N_{GS}$, $M = M_{GS}$ involving a single ("$k$-$\Lambda$ string") bound state. This excitation has been considered previously e.g. in Section 7.7.2 of Ref. 2. It involves having a single (half-odd) integer in the sector corresponding to the set $\{J'^1_\alpha\}$. The lowest-energy bound state which can be created comprises of two $k$s and one $\Lambda$ forming a string pattern in the complex plane. The Takahashi equations describe the real centres of these and other root patterns. The case we consider is realised by the integer configuration

$$I_j = -\frac{N_{GS}-2}{2} - \frac{1}{2} + j, \qquad j = 1, \ldots, N_{GS}-2, \tag{43}$$

$$J^1_\alpha = -\frac{M_{GS}-1}{2} - \frac{1}{2} + \alpha, \qquad \alpha = 1, \ldots, M_{GS}-1, \tag{44}$$

$$J'^1_\beta = J'^p, \qquad \beta = 1, \tag{45}$$

which is displayed in Fig. 4. In the notations used above, we can denote this excited state by $|LWS; \{I_j\}, \{J^1_\alpha\}, \{J'^1_\beta\}\rangle$. We can again take the thermodynamic limit and compare the energy of this excited state with that of the ground state. Following similar manipulations to the case of the ground state energy, the $\mathcal{O}(1)$ corrections can be calculated[2]. The energy is given by

$$E = Le_{\rm GS} + \varepsilon_{k\Lambda}(\Lambda^p) + o(1), \tag{46}$$

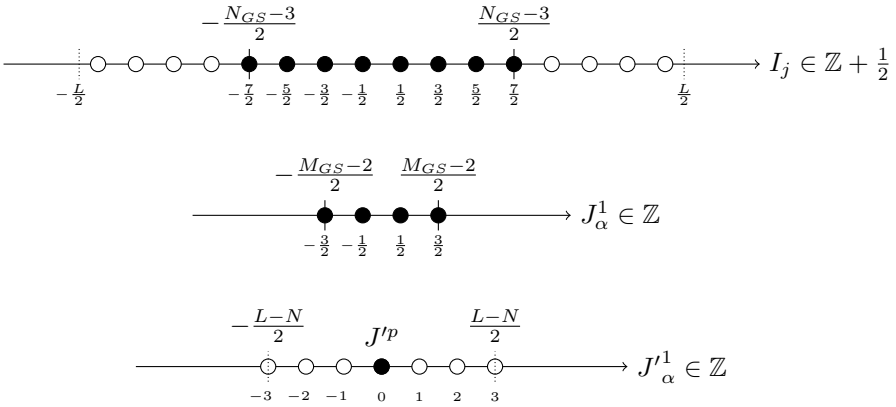


Figure 4: Configuration of the integers for the $k$-$\Lambda$ string excited state

where

$$\varepsilon_{k\Lambda}(\Lambda) = 4\mathrm{Re}\sqrt{1-(\Lambda-iu)^2} - 2\mu - 4u + \int_{-Q}^{Q} dk \cos k \; a_1(\sin k - \Lambda)\; \varepsilon_c(k). \tag{47}$$

The momentum is given by $P = p_{k\Lambda}(\Lambda^p)$, where

$$p_{k\Lambda}(\Lambda') = -2\mathrm{Re}\arcsin(\Lambda'+iu) + \int_{-Q}^{Q} \mathrm{d}k\, \rho_{c,0}(k)\theta\left(\frac{\Lambda'-\sin k}{u}\right), \tag{48}$$

and $\Lambda^p$ is determined by $z_1'(\Lambda^p) = \frac{2\pi J'^p}{L}$. This form can be readily interpreted physically as a particle-like excitation above the ground state. The $k$-$\Lambda$ string dispersion describes the threshold of an excitation continuum obtained by adding e.g. particle-hole excitations in the charge sector. The dispersion relation for this excitation and the particle-hole continuum is shown in Fig. 5. The existence of such a continuum at $p = 0$ is necessary to understand the problem within the mobile impurity approach to threshold singularities.

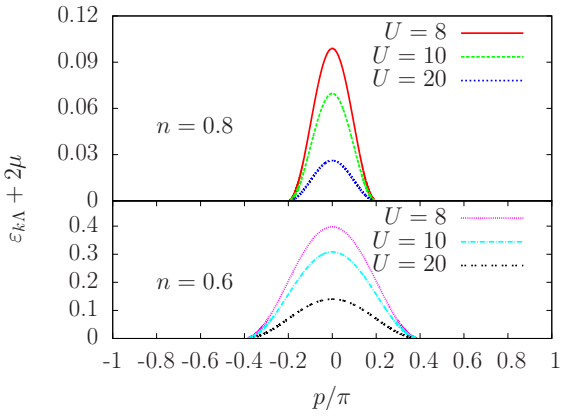


(a) Dispersion relation $\varepsilon_{k\Lambda}(\Lambda(p))$ for the $k$-$\Lambda$ string for various $U$ and $n$. Each curve has been shifted down by $-2\mu$.

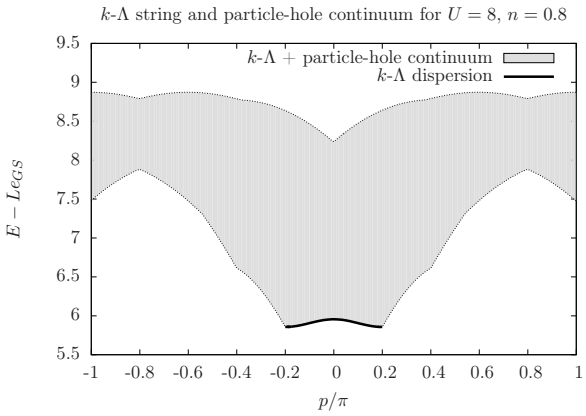


(b) $k$-$\Lambda$ and charge particle-hole excitation continuum.

Figure 5: $k$-$\Lambda$ string dispersion for various $U$ and $n$, and particle-hole excitation continuum above this for $U = 8$, $n = 0.8$. For small momenta, the $k$-$\Lambda$ string dispersion marks the lower edge of a continuum described by additional excitations e.g. particle-hole excitations in the charge sector.

### C. Excitations contributing to $C^{(2)}_{\rm JJ}(\ell,t)$.

We now turn to excited states that contribute to the spectral representation (18) of $C^{(2)}_{\rm JJ}(\ell,t)$. As we have re-expressed $C^{(2)}_{\rm JJ}(\ell,t)$ in terms of matrix elements of the operator $\mathcal{O}^\dagger_j$ defined in (17), we will focus on excited states $|LWS;\mathbf{m}\rangle$ that have non-vanishing matrix elements $\langle GS|\mathcal{O}^\dagger_j|LWS;\mathbf{m}\rangle \neq 0$ These are lowest weight states of the spin and $\eta$-pairing SU(2) algebras and their quantum numbers are $N = N_{GS}-2$, $M = M_{GS}-1$. It is of course straightforward to translate back to excitations contributing to the original spectral representation (15): all that is required is to act with $\eta^\dagger$ on the states we discuss in the following.

#### 1. *"Particle-hole" excitation with $N = N_{GS}-2$, $M = M_{GS}-1$.*

The integer configuration for this type of excitation is given by

$$I_j = \begin{cases} -\frac{N_{GS}}{2} + j + \Theta\left(\frac{-N_{GS}}{2} + j - I^h\right), & j = 1,\ldots,N_{GS}-3 \\ I^p, & j = N_{GS}-2 \end{cases}, \tag{49}$$

$$J_\alpha = -\frac{M_{GS}}{2} + \alpha, \qquad \alpha = 1,\ldots,M_{GS}-1 \quad . \tag{50}$$

This is shown graphically in Fig. 6.

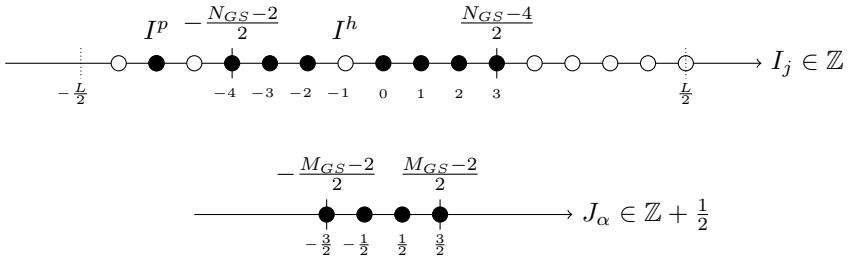


Figure 6: Integer configuration for the particle-hole excitation, explicit numbers for $L = 16$, $N_{GS} = 10$, $M_{GS} = 5$.

In complete analogy to the previous case, the energy and momentum of this state are given by

$$\begin{aligned} E &= Le_{\rm GS} + \varepsilon_c(k^p) - \varepsilon_c(k^h) + o(1), \\ P &= p_c(k^p) - p_c(k^h) \pm 2k_F + o(1), \end{aligned} \tag{51}$$

where $k^p$ and $k^h$ are determined by $z_c(k^p) = \frac{2\pi I^p}{L}$, $z_c(k^h) = \frac{2\pi I^h}{L}$. The contributions $\pm 2k_F$ arise from the asymmetry of the charge "Fermi sea", leaving a choice of two parity-related states. The continuum of excitations given by (51) is shown in Fig. 7, and consists of the union of two copies of the continuum depicted in Fig. 3 shifted by $\pm 2k_F$ respectively. We note that in order to make closer contact with the spectral representation (18) we have shifted the momentum by $\pi$.

#### 2. *"Two particle" excitation with $N = N_{GS}-2$, $M = M_{GS}-1$.*

A closely related type of excitation corresponds to the choice of (half-odd) integers

$$I_j = \begin{cases} -\frac{N_{GS}-4}{2} + j, & j = 1,\ldots,N_{GS}-4 \\ I^{p_1}, & j = N_{GS}-3, \\ I^{p_2}, & j = N_{GS}-2 \end{cases}, \tag{52}$$

$$J_\alpha = -\frac{M_{GS}}{2} + \alpha, \qquad \alpha = 1,\ldots,M_{GS}-1. \tag{53}$$

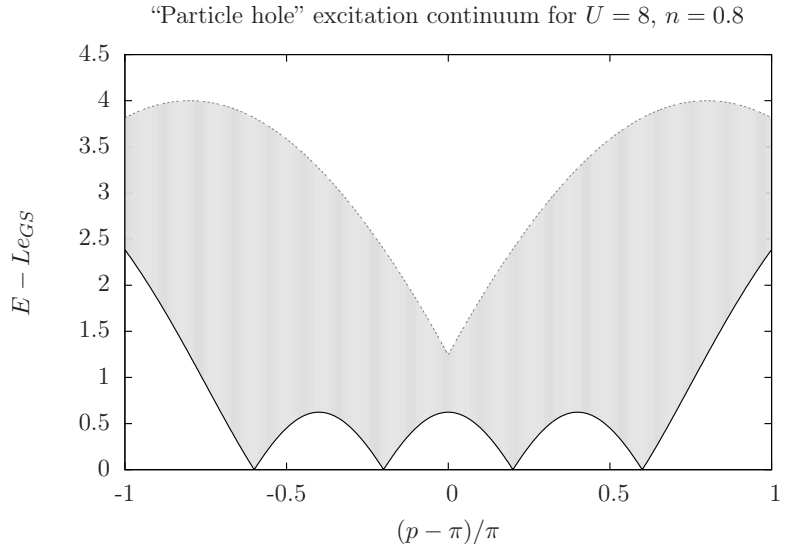


Figure 7: Continuum for particle-hole excitation with momentum shifted for clarity.

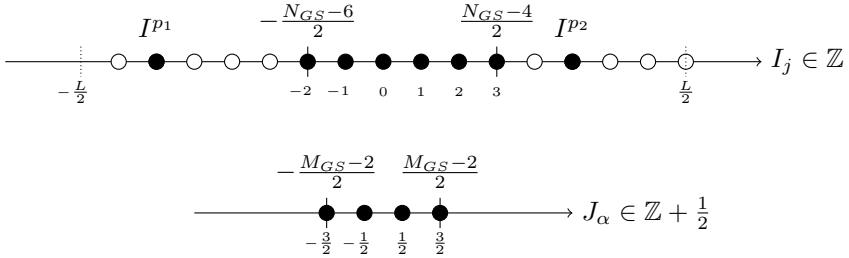


Figure 8: Integer configuration for the particle-particle excitation, explicit numbers for $L = 16$, $N_{GS} = 10$, $M_{GS} = 5$.

Such a configuration is shown in Fig. 8 and can be thought of as involving two particles associated with $I^{p_1}$ and $I^{p_2}$ respectively. The energy and momentum of this excitation are

$$\begin{aligned} E &= Le_{\rm GS} + \varepsilon_c(k^{p_1}) + \varepsilon_c(k^{p_2}) + o(1), \\ P &= p_c(k^{p_1}) + p_c(k^{p_2}) \pm 2k_F + o(1), \end{aligned} \tag{54}$$

with $z_c(k^{p_i}) = \frac{2\pi I^{p_i}}{L}$. The continua corresponding to (54) are shown in Fig. 9. We note that both possible choices $\pm 2k_F$ have been taken into account, and we have again shifted the total momentum by $\pi$ in order to make closer contact with the spectral representation (18) of our correlator.

### *3. "Two hole" excitation with $N = N_{GS} - 2$, $M = M_{GS} - 1$.*

Finally, we consider excitations characterised by the distribution of (half-odd) integers

$$I_j = -\frac{N_{GS}}{2} + j + \Theta\left(-\frac{N_{GS}}{2} + j - I^{h_1}\right) + \Theta\left(-\frac{N_{GS}}{2} + j - I^{h_2}\right), \qquad j = 1, \ldots, N_{GS} - 2, \tag{55}$$

$$J_\alpha = -\frac{M_{GS}}{2} + \alpha, \qquad \alpha = 1, \ldots, M_{GS} - 1, \tag{56}$$

which is displayed in Fig. 10. We see that these states can be viewed as involving two holes associated with $I^{h_1}$ and $I^{h_2}$ respectively. The energy and momentum of this excitation are given by

$$\begin{aligned} E &= Le_{\rm GS} - \varepsilon_c(k^{h_1}) - \varepsilon_c(k^{h_2}) + o(1), \\ P &= -p_c(k^{h_1}) - p_c(k^{h_2}) \pm 2k_F + o(1), \end{aligned} \tag{57}$$

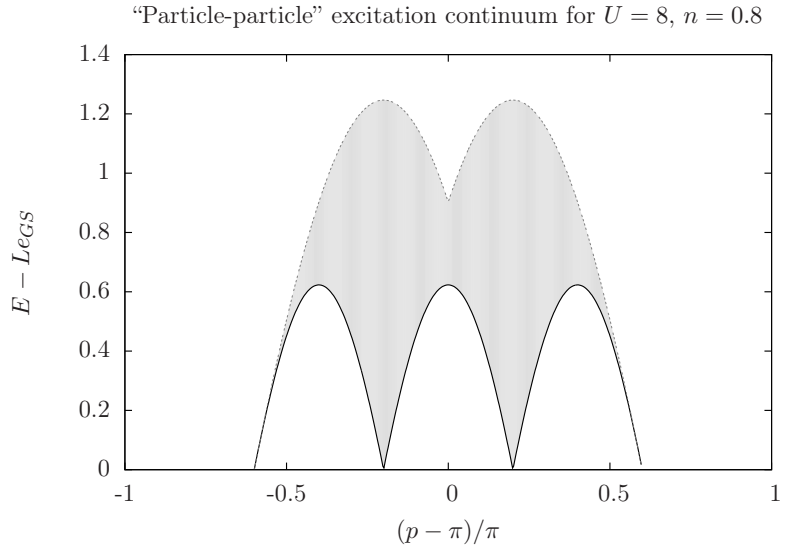


Figure 9: Continuum for particle-particle excitation with momentum shifted for clarity.

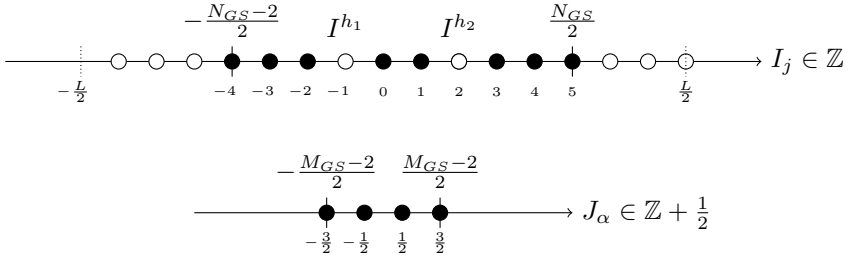


Figure 10: Integer configuration for two hole excited state, explicit numbers for $L = 16$, $N_{GS} = 10$, $M_{GS} = 5$.

with $z_c(k^{h_i}) = \frac{2\pi I^{h_i}}{L}$. The continua for these excitations are shown in Fig. 11, where we have taken both possible choices of $\pm 2k_F$ into account and we again have shifted the total momentum by $\pi$ in order to make closer contact with the spectral representation (18) of our correlator.

### D. Excitation thresholds at commensurate fillings

By considering additional excitations around the "Fermi points" in the charge sector we can construct other excitations that are degenerate in energy (to $o(1)$), but differ in their momenta by integer multiples of $4k_F$. As we consider the case of zero magnetic field, there is no freedom to rearrange the integers in the spin sector that leads to a lower energy for a given momentum. In this way we can determine the thresholds for a given class of excited states.

1. The absolute threshold is obtained by combining the particle-hole excitation of Sec. III B 1 with zero-energy particle-hole excitations at the "Fermi points" in the charge sector, which shift the momentum by multiples of $4k_F$. It is depicted by a dashed red line in Fig. 12. At zero momentum, the relevant value for the optical conductivity, the absolute threshold occurs at zero energy. At low energies the optical conductivity is dominated by particle-hole excitations. Close to half-filling, the spectral weight of this contribution is small and tends to zero for $n \to 1$. In the vicinity of half-filling most of the spectral weight concomitantly occurs above a "pseudo-gap" that is close in value to the Mott gap of the half-filled system.

2. Above an energy scale that tends to the Mott gap as the band filling approaches one from below, excitations involving a single $k$-$\Lambda$ string of length two exist. Their threshold is shown as a dashed black line in Fig. 12. Precisely at half filling these excitations do not contribute to the optical conductivity[2,40,41] as a result of the

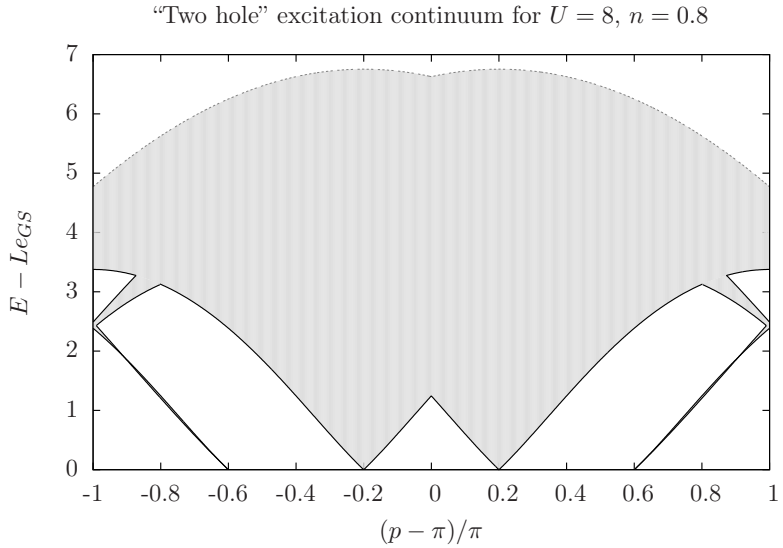


Figure 11: Continuum for two hole excitation with momentum shifted for clarity.

enhanced symmetry: at half filling this excitation describes a singlet of the $\eta$-pairing SU(2) algebra and does not contribute to $\sigma_1(\omega)$.

3. For band fillings close to $n = 1$ there are other excitations of the form $\eta^+|LWS, \mathbf{m}\rangle$ that contribute to the optical conductivity. At half-filling these are the only states contributing to $\sigma_1(\omega)$ in the frequency regime $2\Delta \leq \omega \leq 4\Delta$, where $\Delta$ is the Mott gap. Below half-filling, their contribution to $\sigma_1(\omega)$ can be cast in the form of $C^{(2)}_{\mathrm{JJ}}(\ell, t)$ in (18), and the states to be considered are then given by Sec. III C 1, III C 2 and III C 3.

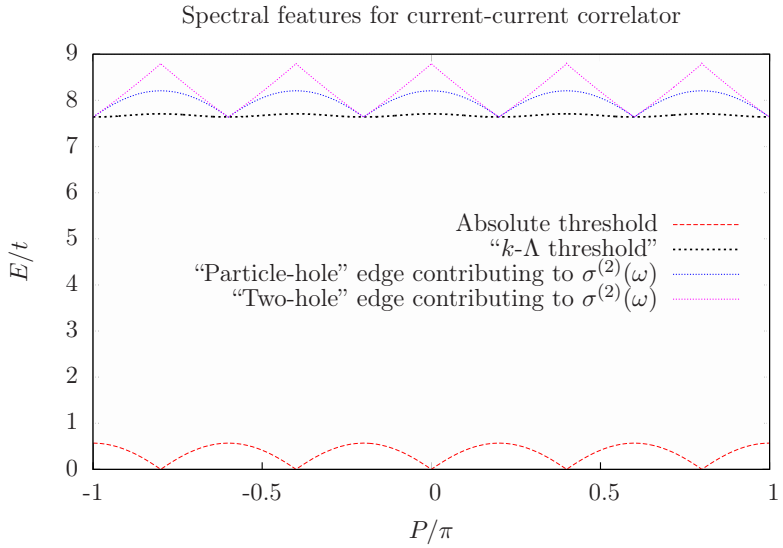


Figure 12: The continuum of lowest-lying excitations of the Hubbard model involving only the charge sector for $n = 0.8$, $U = 10$. As the optical conductivity is defined at zero momentum, only the features encountered at $P = 0$ are relevant. The $k$-$\Lambda$ string dispersion defines the lower edge of a continuum of excitations involving the $k$-$\Lambda$ string. The contributions to $\sigma^{(2)}(\omega)$ are shifted by $-2\mu$, in accordance with the spectral representation (18).

The thresholds shown in Fig. 12 are at a high commensurability: $5(4k_F) = 8\pi$. We note that thresholds involving high-order umklapp processes are suppressed in $\sigma_1(\omega)$, cf. Refs. 10, 14, and 15. Analytic forms for the "high-energy" thresholds are given below in eqns (65), (F1) and (F17). These results show that the contributions from $\sigma^{(2)}(\omega)$

do not constitute the "pseudo-gap threshold", and moreover are suppressed by a factor $1/L$ as we have pointed out before. Hence they do not play an important role in the initial growth of $\sigma_1(\omega)$, even for finite-size systems, and we therefore relegate their discussion to Appendix F.

## IV. MOBILE IMPURITY APPROACH TO THRESHOLD SINGULARITIES

Our goal is to determine the behaviour of the optical conductivity in the metallic phase of the Hubbard model close to half-filling above the excitation thresholds occurring in the vicinity of the Mott gap at $n = 1$. This can be achieved by following the mobile impurity approach to the Hubbard chain set out in Ref. 35. In the main cases of interest to us here, the mobile impurity model describes low-energy degrees of freedom in the presence of a single high-energy excitation with momentum $q$ and takes the general form

$$H = H_{\rm LL} + H_{\rm imp} + H_{\rm int}, \tag{58}$$

$$H_{\rm LL} = \int dx \Big[ \sum_{\alpha=c,s} \frac{v_\alpha}{16\pi} \left( \frac{1}{2K_\alpha} \big(\partial_x \Phi^*_\alpha\big)^2 + 2K_\alpha \big(\partial_x \Theta^*_\alpha\big)^2 \right) \Big], \tag{59}$$

$$H_{\rm imp} = \int {\rm d}x\, B^\dagger(x) \left[ \epsilon(q) - i\epsilon'(q)\partial_x - \frac{1}{2}\epsilon''(q)\partial_x^2 \right] B(x)\ , \tag{60}$$

$$H_{\rm int} = \int dx\ B^\dagger(x) B(x) \left[ f_\alpha(q)\partial_x \varphi^*_\alpha(x) + \bar{f}_\alpha(q)\partial_x \bar{\varphi}^*_\alpha(x) \right] + \dots\ . \tag{61}$$

Here $v_{c,s}$ and $K_{c,s}$ are respectively the velocities and Luttinger parameters of low-energy collective spin and charge degrees of freedom, $\varphi^*_{c,s}$, $\bar{\varphi}^*_{c,s}$ are chiral charge and spin Bose fields, and

$$\Phi^*_\alpha = \varphi^*_\alpha + \bar{\varphi}^*_\alpha\ , \quad \Theta^*_\alpha = \varphi^*_\alpha - \bar{\varphi}^*_\alpha\ , \qquad \alpha = c, s. \tag{62}$$

The high-energy excitation under consideration has a "bare" dispersion $\epsilon(q)$ and is described in terms of the field $B(x)$. Finally, the functions $f_{c,s}(q)$ and $\bar{f}_{c,s}(q)$ parametrise the interactions between the high-energy excitation and the low-energy degrees of freedom. Our Bose fields are related to the usual spin and charge bosons[7,8] by a canonical transformation

$$\Phi_\alpha = \frac{\Phi^*_\alpha}{\sqrt{2}}\ , \quad \Theta_\alpha = \sqrt{2}\Theta^*_\alpha\ , \tag{63}$$

and were introduced in Ref. 35 by bosonizing the physical fermionic spin and charge excitations in the Hubbard model. The form of $H_{\rm int}$ is fixed by symmetry considerations and assuming the high-energy excitation to be a point-like object. Within the mobile impurity model the current operator is represented as

$$J_j \to B^\dagger(x)\mathcal{O}_{\rm LL}(x), \tag{64}$$

where $\mathcal{O}_{\rm LL}(x)$ is an operator acting in the Luttinger liquid sector of the model (61) only. In order to fully specify our problem we proceed as follows:

1. The spin and charge velocities and Luttinger parameters are determined directly from the exact solution of the Hubbard model, see Appendix A for a brief summary.

2. The relevant ("dressed") dispersion relations for the various excitations we need to consider have already been determined above in section III.

3. For a given threshold, the projection $\mathcal{O}_{\rm LL}$ of the current operator onto the Luttinger liquid sector is determined by bosonisation/refermionisation techniques. This is done in sections IV A 1, F 1 a and F 2 a below.

4. Finally, the interaction parameters $f_{c,s}(q)$, $\bar{f}_{c,s}(q)$ are determined in sections IV A 4, F 1 d and F 2 d by comparing finite-size corrections to excitation energies in the Hubbard model and the mobile impurity model (58).

### A. $k$-$\Lambda$ threshold in $\sigma^{(1)}(\omega)$

This threshold is obtained when the entire $\mathcal{O}(1)$ contribution to the excitation energy and momentum are carried by the $k$-$\Lambda$ string. The functional form of the threshold is

$$E^{k\text{-}\Lambda}_{\text{thres}}(q) = \varepsilon_{k\Lambda}\big(\Lambda(q)\big),$$
$$q = -2\,\text{Re}\,\arcsin(\Lambda + iu) + \int_{-Q}^{Q} dk\,\theta\left(\frac{\Lambda - \sin k}{u}\right)\rho_{c,0}(k), \tag{65}$$

where $\rho_{c,0}(k)$ is the ground state root density (32). It important to note that in the case relevant for the optical conductivity the $k$-$\Lambda$ string sits at $q = 0$, which corresponds to a *maximum* of $\varepsilon_{k\Lambda}(\Lambda)$. The mobile impurity Hamiltonian appropriate for the description of this case is therefore of the form

$$H_{\text{imp}} = \int \mathrm{d}x\, B^\dagger(x)\left(\epsilon(0) - \frac{1}{2}\epsilon''(0)\partial_x^2\right)B(x), \tag{66}$$

where $\epsilon''(0) < 0$. We note that by virtue of the interactions between the mobile impurity and the Luttinger liquid degrees of freedom, the bare dispersion $\epsilon(q)$ is differs from the actual threshold $\varepsilon_{k\Lambda}\big(\Lambda(q)\big)$. The relationship between the two quantities is established below. The threshold $\varepsilon_{k\Lambda}(0)$ is shown in Fig. 13 for various $U$ and $n$

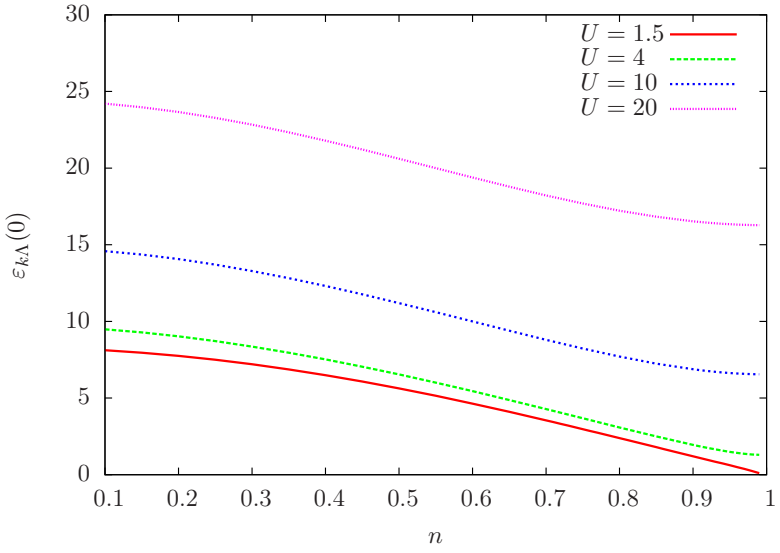


Figure 13: The threshold of the $k$-$\Lambda$ string $\varepsilon_{k\Lambda}(0)$ is shown for various $U$ and $n$

#### 1. *Projection of the current operator*

Having identified the state involving the $k$-$\Lambda$ string as contributing to $\sigma_1^{(1)}(\omega)$, we wish to project the current operator (7) onto the operators involved in the mobile impurity model. To this end we introduce the Hubbard projection operators[2], defined on site $j$ as

$$X_j^{ab} := |a\rangle_{jj}\langle b|, \qquad a, b = 0, \uparrow, \downarrow, 2\,(\uparrow\downarrow). \tag{67}$$

The current operator is expressed in terms of the $X_j^{ab}$ as

$$J_j = -it\sum_\sigma \left(\sigma X_j^{2\bar\sigma} + X_j^{\sigma 0}\right)\left(\sigma X_{j+1}^{\bar\sigma 2} + X_{j+1}^{0\sigma}\right) - \left(\sigma X_{j+1}^{2\bar\sigma} + X_{j+1}^{\sigma 0}\right)\left(\sigma X_j^{\bar\sigma 2} + X_j^{0\sigma}\right). \tag{68}$$

In order to proceed further, we now consider the large-$U$ limit, in which the $k$-$\Lambda$ string corresponds to a doubly-occupied site. The current operator $J$ can be decomposed into three terms: a piece which increases the double occupancy by one ($J^+$), a piece which decreases it by one ($J^-$) and a piece that leaves the double occupancy unchanged ($J^0$) i.e.

$$J_j = J_j^+ + J_j^- + J_j^0\ . \tag{69}$$

As we are concerned with creating an excitation involving double-occupation, we are interested in $J_j^+$ only. This is given by

$$J_j^+ = -it\sum_\sigma \sigma X_j^{2\bar\sigma} X_{j+1}^{0\sigma} - \sigma X_{j+1}^{2\bar\sigma} X_j^{0\sigma}, \tag{70}$$

and can be suggestively rewritten as

$$J_j^+ = -it\left[X_j^{20}\left(X_j^{0\downarrow}X_{j+1}^{0\uparrow} - X_j^{0\uparrow}X_{j+1}^{0\downarrow}\right) - X_{j+1}^{20}\left(X_{j+1}^{0\downarrow}X_j^{0\uparrow} - X_{j+1}^{0\uparrow}X_j^{0\downarrow}\right)\right]. \tag{71}$$

As, in the large-$U$ limit, a $k$-$\Lambda$ string corresponds to a doubly occupied site, while the ground state has zero double occupancy, we can identify the operator creating the $k$-$\Lambda$ string as $B^\dagger(x) \sim X_j^{20}$. This allows us to recast $J^+$ in the form

$$J_j^+ \sim -it\left[B_j^\dagger - B_{j+1}^\dagger\right]\left(c_{j,\downarrow}c_{j+1,\uparrow}\left(1-n_{j,\uparrow}\right)\left(1-n_{j+1,\downarrow}\right) - c_{j,\uparrow}c_{j+1,\downarrow}\left(1-n_{j,\downarrow}\right)\left(1-n_{j+1,\uparrow}\right)\right). \tag{72}$$

In order to complete the projection of the current operator onto the mobile impurity model we simply bosonize all remaining electron operators. The final result is

$$J_{k\Lambda}(x) \sim \left(\partial_x B^\dagger(x)\right) e^{-i\Theta_c^*(x)/\sqrt{2}} \sin\left(\frac{\Phi_s^*}{2\sqrt{2}}\right) + \dots \tag{73}$$

### *2. Finite-size corrections to excitation energies in the mobile impurity model*

Energies of excited states in the mobile impurity model in a large, finite volume can be calculated following Refs. 20 and 35. The chiral spin and charge Bose fields have mode expansions

$$\varphi_\alpha^*(x) = \varphi_{\alpha,0}^* + \frac{x}{L}Q_\alpha^* + \sum_{n=1}^\infty \sqrt{\frac{2}{n}}\left[e^{i\frac{2\pi n}{L}x}a_{\alpha,R,n} + e^{-i\frac{2\pi n}{L}x}a_{\alpha,R,n}^\dagger\right], \tag{74}$$

$$\bar\varphi_\alpha^*(x) = \bar\varphi_{\alpha,0}^* + \frac{x}{L}\bar Q_\alpha^* + \sum_{n=1}^\infty \sqrt{\frac{2}{n}}\left[e^{-i\frac{2\pi n}{L}x}a_{\alpha,L,n} + e^{i\frac{2\pi n}{L}x}a_{\alpha,L,n}^\dagger\right]. \tag{75}$$

Here $Q_\alpha^*$, $\bar Q_\alpha^*$, $\varphi_{\alpha,0}$, $\bar\varphi_{\alpha,0}$ are zero-mode operators, obeying the commutation relations

$$[\varphi_{\alpha,0}^*, Q_\alpha^*] = -[\bar\varphi_{\alpha,0}^*, \bar Q_\alpha^*] = -4\pi i. \tag{76}$$

The eigenvalues $q_\alpha$, $\bar q_\alpha$ of the operators $Q_\alpha^*$, $\bar Q_\alpha^*$ depend on the boundary conditions of the fields $\varphi_\alpha^*(x)$, $\bar\varphi_\alpha^*(x)$. These boundary conditions are, crucially, influenced by the presence of a mobile impurity: coupling the impurity to the Luttinger liquid will change the boundary conditions and therefore modify the eigenvalue spectrum, causing a shift in the $\mathcal{O}(L^{-1})$ spectrum. It is precisely this relationship that will allow us to determine the coupling constants by examining the finite-size spectrum of the Hubbard model in the presence of a high-energy excitation. An important distinction from previous calculations is that the dispersion of the mobile impurity is quadratic in our case and has negative curvature.

The interactions between the impurity and the LL degrees of freedom in (58) can be removed by a unitary transformation of the form[35,36]

$$U = e^{-i\int_{-\infty}^\infty dx\ \sum_\alpha(\gamma_\alpha\varphi_\alpha^*(x) + \bar\gamma_\alpha\bar\varphi_\alpha^*(x))B^\dagger(x)B(x)}. \tag{77}$$

The transformed fields are given by

$$\begin{aligned}
\varphi_\alpha^\circ &= U\varphi_\alpha^* U^\dagger = \varphi_\alpha^*(x) - 2\pi\gamma_\alpha C(x),\\
\bar\varphi_\alpha^\circ &= U\bar\varphi_\alpha^* U^\dagger = \bar\varphi_\alpha^*(x) + 2\pi\bar\gamma_\alpha C(x),\\
\widetilde{B}(x) &= UB(x)U^\dagger = B(x)e^{i\sum_\alpha(\gamma_\alpha\varphi_\alpha^*(x) + \bar\gamma_\alpha\bar\varphi_\alpha^*(x))}e^{-i\pi\sum_\alpha(\gamma_\alpha^2 - \bar\gamma_\alpha^2)C(x)},
\end{aligned} \tag{78}$$

where

$$C(x) = \int_{-\infty}^\infty \mathrm{d}y\,\mathrm{sgn}(x-y)B^\dagger(y)B(y). \tag{79}$$

By choosing the parameters $\gamma_\alpha$, $\bar{\gamma}_\alpha$ to fulfil

$$\begin{pmatrix} f_\alpha \\ \bar{f}_\alpha \end{pmatrix} = \begin{pmatrix} -v_\alpha^+ & -v_\alpha^- \\ v_\alpha^- & v_\alpha^+ \end{pmatrix} \begin{pmatrix} \gamma_\alpha \\ \bar{\gamma}_\alpha \end{pmatrix}, \qquad v_\alpha^\pm = \frac{v_\alpha}{2}\left(2K_\alpha \pm \frac{1}{2K_\alpha}\right), \tag{80}$$

we find that, retaining only the most relevant terms, the impurity decouples in the new basisi.e.

$$H = \int \mathrm{d}x \left[\sum_{\alpha=c,s} \frac{v_\alpha}{16\pi}\left(\frac{1}{2K_\alpha}\left(\partial_x \Phi_\alpha^\circ\right)^2 + 2K_\alpha\left(\partial_x \Theta_\alpha^\circ\right)^2\right)\right] + \int \mathrm{d}x\, \widetilde{B}^\dagger(x)\left[\widetilde{\epsilon}(q) - \frac{1}{2}\widetilde{\epsilon}''(q)\partial_x^2\right]\widetilde{B}(x) + \ldots. \tag{81}$$

We note that the "dressed" impurity dispersion for momenta $k \approx q$ is $\widetilde{\epsilon}(q) - \frac{1}{2}\widetilde{\epsilon}''(q)(k-q)^2$ and differs from its "bare" value $\epsilon(k)$ by a constant[37]. Importantly, it is the *dressed* dispersion that relates directly to the Bethe Ansatz result for $E^{k\text{-}\Lambda}_{\text{thres}}(k)$ in (65). In the decoupled theory of (81) it is a straightforward matter to calculate the spectrum of *low-energy* excitations above the ground state in the presence of an impurity. The result is[35]

$$\Delta E_{LL} = \sum_{\alpha=c,s} \frac{2\pi v_\alpha}{L}\left[\frac{1}{4K_\alpha}\left(\frac{q_\alpha + \bar{q}_\alpha}{4\pi} - \gamma_\alpha + \bar{\gamma}_\alpha\right)^2 + K_\alpha\left(\frac{q_\alpha - \bar{q}_\alpha}{4\pi} - \gamma_\alpha - \bar{\gamma}_\alpha\right)^2 + \sum_{n>0} n\left[M_{n,\alpha}^+ + M_{n,\alpha}^-\right]\right]. \tag{82}$$

Here $M_{n,\alpha}^\pm$ are non-negative integers corresponding to particle-hole excitations at the edge of the "Fermi seas". Any operator acting on the ground state will, in general, produce a superposition of energy eigenstates. Noting that the ground state is annihilated by $Q_\alpha^*$, $\bar{Q}_\alpha^*$, the state $\mathcal{O}(x)|GS\rangle$ has well-defined quantum numbers $q_\alpha^{(0)}$, $\bar{q}_\alpha^{(0)}$ if $\mathcal{O}(x)$ satisfies the relations

$$[Q_\alpha^*, \mathcal{O}(x)] = q_\alpha^{(0)}\mathcal{O}(x), \qquad [\bar{Q}_\alpha^*, \mathcal{O}(x)] = \bar{q}_\alpha^{(0)}\mathcal{O}(x). \tag{83}$$

If the operator satisfies such a property then all states in the superposition defined by $\mathcal{O}(x)|GS\rangle$ must have the *same* $q_\alpha$, $\bar{q}_\alpha$, namely $q_\alpha^{(0)}$, $\bar{q}_\alpha^{(0)}$. The only difference in the energies comes from having different $M_{n,\alpha}^\pm$. We can therefore identify the "minimal" excitation[35]: this is the state with all $M_{n,\alpha}^\pm = 0$ i.e. no particle-hole excitations. For the specific case of interest here, namely acting with the projected current operator $J_{k\Lambda}(x)$ on the ground state, this can be represented pictorially as

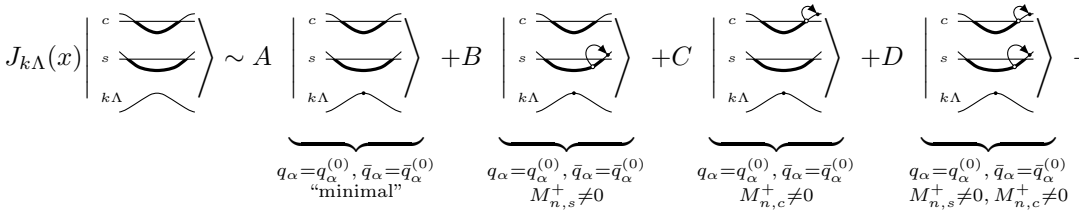


From the bosonised expression for $J_{k\Lambda}(x)$, and focussing only on the $e^{i\Phi_s^*/2\sqrt{2}}$ term with the other following from parity, it follows that

$$q_c^{(0)} = \bar{q}_c^{(0)} = 2\pi\sqrt{2}; \qquad q_s^{(0)} = -\bar{q}_s^{(0)} = -\pi\sqrt{2}. \tag{85}$$

The total momentum can also be calculated using the mode expansion, and is found to be of the form

$$P = \frac{k_F}{\pi\sqrt{2}}\left(\bar{q}_c - q_c\right) + P_{\text{imp}}(k_L^p) + \frac{2\pi}{L}\sum_{\alpha=c,s}\left[\left(\frac{q_\alpha + \bar{q}_\alpha}{4\pi} - \gamma_\alpha + \bar{\gamma}_\alpha\right)\left(\frac{q_\alpha - \bar{q}_\alpha}{4\pi} - \gamma_\alpha - \bar{\gamma}_\alpha\right) + \left(N_\alpha^+ - N_\alpha^-\right)\right], \tag{86}$$

where $k_L^p$ includes finite-size shifts to the rapidity $k^p$. We can identify the "minimally excited" state with the Bethe Ansatz excitation at the relevant threshold. By matching the expressions for the finite-size energies, we will be able to constrain the parameters $\gamma_\alpha$, $\bar{\gamma}_\alpha$.

### *3. Finite-size corrections to excitation energies from Bethe Ansatz*

Finite-size corrections to the energies of states involving both high- and low-energy excitations can be determined from the Bethe Ansatz solution of the Hubbard model following Ref. 25. The details for the excitations of interest

here involving a $k$-$\Lambda$ string are given in Appendix B. The final result for zero magnetic field and total momentum $P = \mathcal{O}(L^{-1})$ is

$$E = e_{GS}L + \varepsilon_{k\Lambda}(0) - \frac{\pi}{6L}(v_c + v_s) + \frac{2\pi v_c}{L}\left[\frac{(\Delta N_c - N_c^{\rm imp})^2}{8K_c} + 2K_c\left(D_c - D_c^{\rm imp} + \frac{D_s - D_s^{\rm imp}}{2}\right)^2\right] + \frac{2\pi v_s}{L}\left[\frac{1}{2}\left(\Delta N_s - \frac{\Delta N_c}{2}\right)^2 + \frac{(D_s - D_s^{\rm imp})^2}{2}\right]. \quad (87)$$

Here $e_{GS}$ is the ground state energy per site in the thermodynamic limit, while $\varepsilon_{k\Lambda}(0)$ is the contribution due to the (high-energy) $k$-$\Lambda$ string excitation and is obtained from the solution of the integral equations

$$\varepsilon_{k\Lambda}(\Lambda) = 4{\rm Re}\sqrt{1-(\Lambda - iu)^2} - 2\mu - 4u + \int_{-Q}^{Q} {\rm d}k\, \cos k\, a_1(\sin k - \Lambda)\, \varepsilon_c(k),$$
$$\varepsilon_c(k) = -2\cos k - \mu - 2u + \int_{-Q}^{Q} {\rm d}k'\ \cos k'\, R(\sin k - \sin k')\varepsilon_c(k'), \quad (88)$$

where the function $R(x)$ is given by

$$R(x) = \int_{-\infty}^{\infty} \frac{d\omega}{2\pi} \frac{e^{i\omega x}}{1 + \exp(2u|\omega|)}. \quad (89)$$

The spin and charge velocities $v_{s,c}$ and the Luttinger parameter $K_c$ are given in Appendix A, while the quantities $N_c^{\rm imp}$ and $D_{c,s}^{\rm imp}$ are given by

$$D_c^{\rm imp} = 0, \quad D_s^{\rm imp} = 0\ , \quad N_c^{\rm imp} = \int_{-Q}^{Q} {\rm d}k\, \rho_{c,1}(k), \quad (90)$$

where

$$\rho_{c,1}(k) = \cos k\, a_1(\sin k - \Lambda'^p) + \cos k \int_{-Q}^{Q} dk'\ \rho_{c,1}(k')R(\sin k - \sin k'). \quad (91)$$

Finally, the quantities $\Delta N_c$, $\Delta N_s$, $D_c$ and $D_s$ characterise low-energy excitations of the spin and charge degrees of freedom and for the "minimal" excitation of interest are given by

$$\Delta N_c = -2\ , \quad D_c = 0\ , \quad \Delta N_s = -1\ , \quad D_s = 0. \quad (92)$$

We note that in order to fully specify the mobile impurity model we require the value of the curvature of the impurity dispersion at its maximum. This is given by

$$\frac{1}{m} = \left.\frac{\partial^2 \varepsilon_{k\Lambda}(\Lambda)}{\partial p^2}\right|_{\Lambda=0} = \frac{\varepsilon''_{k\Lambda}(0)}{(2\pi\sigma_1'^h(0))^2}, \quad (93)$$

where

$$\varepsilon''_{k\Lambda}(0) = -\frac{4}{(1+u^2)^{3/2}} - \int_{-Q}^{Q} {\rm d}k\, a_1'(\sin k)\varepsilon_c'(k),$$
$$2\pi\sigma_1'^h(0) = \frac{2}{\sqrt{1+u^2}} - 2\pi\int_{-Q}^{Q} {\rm d}k\, a_1(\sin k)\rho_{c,0}(k). \quad (94)$$

The total momentum of the state of interest can also be calculated from the Bethe Ansatz and for the case of interest results in

$$P = q_L + 2k_F(2D_c + D_s) + \frac{2\pi}{L}\sum_{\alpha=c,s}\left[(\Delta N_\alpha - N_\alpha^{\rm imp})(D_\alpha - D_\alpha^{\rm imp}) + (N_\alpha^+ - N_\alpha^-)\right], \quad (95)$$

with $q_L$ the contribution, including finite-size shifts of the rapidities, from the high-energy impurity and $N_\alpha^\pm$ are integers corresponding to particle-hole pairs at the edge of the "Fermi seas". The method used for deriving this result is summarised in Appendix E.

### 4. Fixing the parameters $\gamma_\alpha$, $\bar{\gamma}_\alpha$

By equating the Bethe Ansatz results (87) and (95) for energy and momentum with the ones obtained in the framework of the mobile impurity model (82), (86) we can fix the parameters $\gamma_\alpha$, $\bar{\gamma}_\alpha$ to be

$$\gamma_c = -\bar{\gamma}_c = \frac{1}{\sqrt{2}} + \frac{(\Delta N_c - N_c^{\rm imp})}{2\sqrt{2}}; \qquad \gamma_s = \bar{\gamma}_s = -\frac{1}{2\sqrt{2}}. \tag{96}$$

### 5. Current-current correlator in the mobile impurity model

We are now in a position to work out the current-current correlation function (15) in the mobile impurity model framework. Given the expression (73) for the projection of the current operator, we have

$$C^{(1)}_{\rm JJ}(\ell,t) \sim G(x,t) = \langle J^\dagger_{k\Lambda}(x,t) J_{k\Lambda}(0,0)\rangle. \tag{97}$$

In order to evaluate $G(x,t)$ we go over to the transformed basis, in which the impurity decouples from the LL degrees of freedom. Given (96), the leading contribution takes the form

$$\begin{aligned} J_{k\Lambda}(x) \sim\ & \partial_x \widetilde{B}^\dagger(x) e^{i\Theta_c^\circ(x)\frac{\Delta N_c - N_c^{\rm imp}}{2\sqrt{2}}} + i\gamma_c \widetilde{B}^\dagger(x)\partial_x\Theta_c^\circ(x) e^{i\Theta_c^\circ(x)\frac{\Delta N_c - N_c^{\rm imp}}{2\sqrt{2}}} \\ & - \frac{i}{2\sqrt{2}} \widetilde{B}^\dagger(x)\partial_x\Phi_s^\circ(x) e^{i\Theta_c^\circ(x)\frac{\Delta N_c - N_c^{\rm imp}}{2\sqrt{2}}}. \end{aligned} \tag{98}$$

Substituting this back into (97) leads to three kinds of contributions to the correlator

$$\begin{aligned} G(x,t) =\ & G_1(x,t)\langle \partial_x\widetilde{B}(x,t)\partial_x\widetilde{B}^\dagger(0,0)\rangle + G_2(x,t)\langle \widetilde{B}(x,t)\widetilde{B}^\dagger(0,0)\rangle \\ & + G_3(x,t) i\left[\langle \partial_x\widetilde{B}(x,t)\widetilde{B}^\dagger(0,0) - \langle \widetilde{B}(x,t)\partial_x\widetilde{B}^\dagger(0,0)\right]. \end{aligned} \tag{99}$$

Here $G_j(x,t)$ are correlation functions in the LL sector of the theory and can be evaluated by standard methods. The results are

$$\begin{aligned} G_1(x,t) &= \frac{1}{(x^2 - v_c^2 t^2)^\gamma}\ , \\ \frac{G_2(x,t)}{G_1(x,t)} &= -\frac{2\gamma_c^2}{K_c}\left[\frac{x^2+v_c^2t^2}{(x^2-v_c^2t^2)^2} + \frac{2\gamma x^2}{(x^2-v_c^2t^2)^2}\right] - \frac{1}{2}\frac{x^2+v_s^2t^2}{(x^2-v_s^2t^2)^2}\ , \\ \frac{G_3(x,t)}{G_1(x,t)} &= i\gamma_c\sqrt{\frac{\gamma}{K_c}}{\rm sgn}(N_c^{\rm imp}+2)\ \frac{2x}{x^2-v_c^2t^2}\ , \end{aligned} \tag{100}$$

where we have defined

$$\gamma = \frac{1}{2K_c}\left(1 + \frac{N_c^{\rm imp}}{2}\right)^2. \tag{101}$$

The free impurity correlator is given by

$$\langle \widetilde{B}(x,t)\widetilde{B}^\dagger(0,0)\rangle = \int_{-\Lambda}^{\Lambda}\frac{{\rm d}p}{2\pi} e^{-ipx} e^{-i\varepsilon(p)t}, \tag{102}$$

where $\varepsilon(p)$ is the dispersion relation for the $k$-$\Lambda$ string and $\Lambda$ is a momentum cutoff for the impurity excitation. Using (97), (99), (100) and (102) we may now determine the contribution from the $k$-$\Lambda$ string excitation to the retarded correlator (6). The result can be written in the form

$$\begin{aligned} \sigma_1(\omega)\Big|_{k\Lambda} \sim \frac{1}{\omega}\int_{-\Lambda}^{\Lambda}{\rm d}p \Bigg\{ & \frac{\gamma_c^2}{K_c}\Big((1+\gamma)\Big[\widetilde{G}^c_{\gamma+2,\gamma}\big(\omega-\varepsilon(p),p\big) + \widetilde{G}^c_{\gamma,\gamma+2}\big(\omega-\varepsilon(p),p\big)\Big] - 2\gamma\widetilde{G}^c_{\gamma+1,\gamma+1}\big(\omega-\varepsilon(p),p\big)\Big) \\ & + \sqrt{\frac{4\gamma}{K_c}}\gamma_c p\Big[\widetilde{G}^c_{\gamma+1,\gamma}\big(\omega-\varepsilon(p),p\big) - \widetilde{G}^c_{\gamma,\gamma+1}\big(\omega-\varepsilon(p),p\big)\Big] + p^2\widetilde{G}^c_{\gamma,\gamma}\big(\omega-\varepsilon(p),p\big) \\ & + \gamma_s^2\Big[\widetilde{G}^s_{\gamma}\big(\omega-\varepsilon(p),p\big) + \widetilde{G}^s_{\gamma}\big(\omega-\varepsilon(p),-p\big)\Big]\Bigg\}, \end{aligned} \tag{103}$$

where we have defined

$$\widetilde{G}^{c}_{\gamma_+,\gamma_-}(\omega,p)=\frac{(2\pi)^2}{\Gamma(\gamma_+)\Gamma(\gamma_-)(2v_c)^{\gamma_++\gamma_--1}}(\omega+v_cp)^{\gamma_+-1}(\omega-v_cp)^{\gamma_--1}\Theta(\omega-v_c|p|)\ , \tag{104}$$

$$\begin{aligned}\widetilde{G}^{s}_{\gamma}(\omega,p)=&\int_0^1 \mathrm{d}s\left[\frac{2\pi}{\Gamma(\gamma)}\right]^2\frac{(\omega-v_sp)^{2\gamma-1}}{(v_c^2-v_s^2)^{\gamma}}\Theta(\omega-v_sp)s^{\gamma-1}(1-s)^{\gamma-1}\\&\times\left[\frac{2v_c(\omega-v_sp)}{v_c^2-v_s^2}s-\frac{\omega-v_cp}{v_c-v_s}\right]\Theta\Big(\frac{2v_c(\omega-v_sp)}{v_c^2-v_s^2}s-\frac{\omega-v_cp}{v_c-v_s}\Big).\end{aligned} \tag{105}$$

The dependence of (103) on the momentum cutoff $\Lambda$ is shown in Fig. 14. We see that over a wide range the result is only weakly cutoff-dependent. Unfortunately, the mobile impurity method provides no simple way of predicting how large the cutoff should be. The only obvious constraint is that it should fulfil $\Lambda \ll \pi(1-n)$. If we approach the threshold from above, i.e. consider the limit $\omega \to \varepsilon_{k\Lambda}(0)$, the remaining integral in (103) can be carried out and yields a power-law behaviour of the form

$$\lim_{\omega\to\varepsilon_{k\Lambda}(0)}\sigma_1(\omega)\Big|_{k\Lambda}\sim\frac{1}{\omega}\left[\omega-\varepsilon_{k\Lambda}(0)\right]^{\gamma-1}\Theta\left(\omega-\varepsilon_{k\Lambda}(0)\right). \tag{106}$$

This is shown in Fig. 14 together with numerical evaluations of (103) for several values of the cutoff $\Lambda$, and is seen to provide a good approximation across the entire frequency range examined. Importantly, the exponent $\gamma-1$ is always larger than one, which is in disagreement with that of Ref. 50 . Additionally, the exponent $\gamma$ can be calculated for a

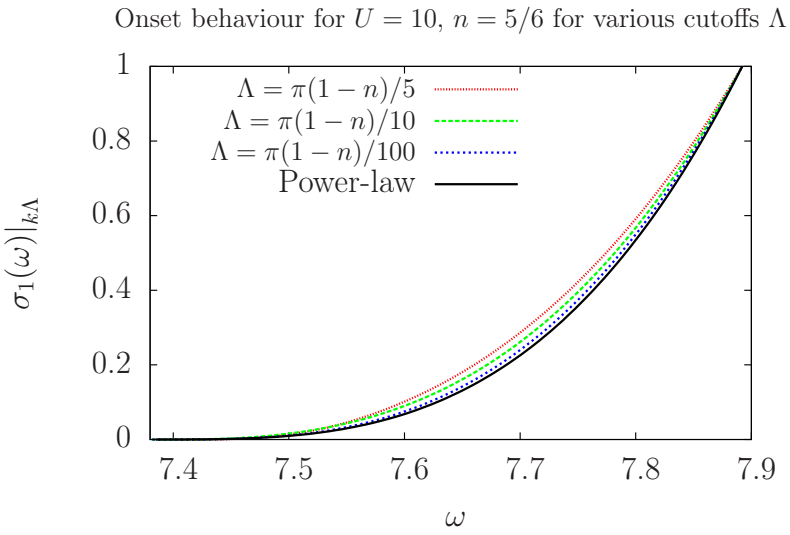


Figure 14: Optical conductivity (103) for $U=10$, $n=5/6$ and several values of the cutoff $\Lambda$. The different curves have been normalized such that $\sigma_1(\varepsilon_{k\Lambda}+0.5)\Big|_{k\Lambda}=1$. For comparison we show the power-law behaviour (106), valid for $\omega\to\varepsilon_{k\Lambda}$. We see that the power law in fact provides a good approximation over the entire range of comparison.

variety of parameters, as presented in Fig. 15.

## V. COMPARISON WITH NUMERICAL RESULTS

In Ref. 59 the optical conductivity of the one dimensional Hubbard model has been computed by matrix product methods. The approach requires introduction of a damping parameter $\eta>0$ and provides Im $\chi^J(\omega+i\eta)$ for a chain of finite length. In order to facilitate a comparison with the results obtained here it is necessary to remove this broadening. In order to do this approximately we proceed as follows. For positive frequencies the zero temperature

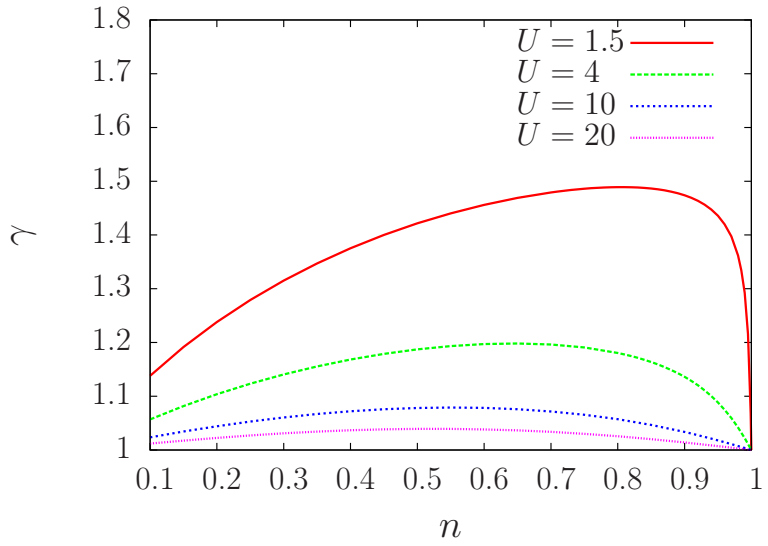


Figure 15: Value of the exponent $\gamma$ in (106) characterizing the power-law behaviour of $\sigma_1(\omega)$ just above the pseudo-gap, for several values of $U$ and $n$

optical conductivity can be expressed as

$$\sigma_1(\omega > 0) = -\frac{\text{Im}\ \chi_+(\omega)}{\omega} \ ,$$
$$\chi_+(\omega) = \frac{e^2}{L} \sum_n \frac{|\langle \text{GS}|J|n\rangle|^2}{\omega + i0 - E_n + E_{\text{GS}}} \ . \tag{107}$$

Ref. 59 provides results for the quantity

$$\chi_+(\omega; L, \eta) = \int_{-\infty+i0}^{\infty+i0} \frac{d\omega'}{2\pi} \ \frac{2\eta}{\eta^2 + (\omega - \omega')^2} \text{Im}\ \chi_+(\omega') \ , \tag{108}$$

where $L$ is the chain length and $\omega$ takes values on a regular grid of frequencies. We first use rational function interpolation to extract a continuous function from the numerical data, which we then deconvolve using the Richardson-Lucy algorithm[60,61].

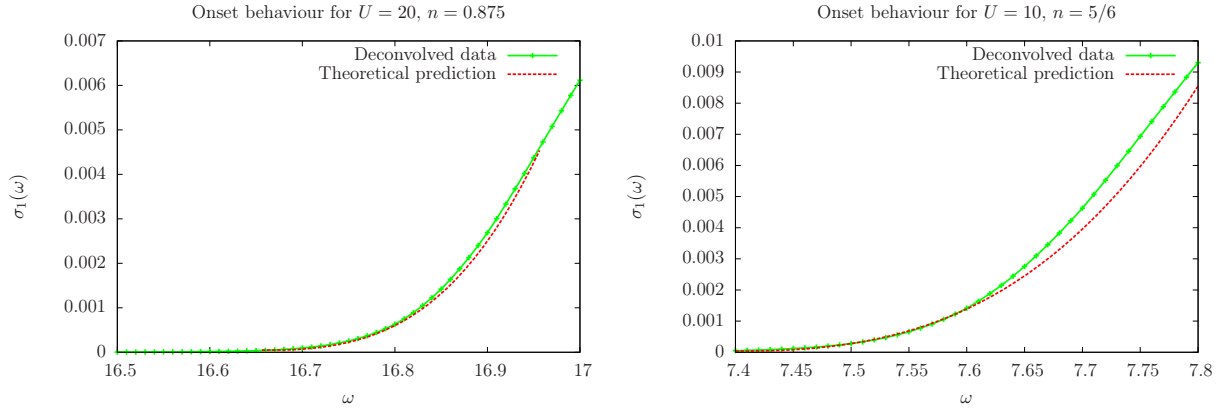


Figure 16: Comparison of deconvolved DMRG data with the onset as predicted in (103), varying the offset and overall scale factor and choosing $\Lambda = (1 - n)\pi/10$.

The deconvolved numerical results obtained in this way can then be compared to the onset predicted at the lowest threshold, as given by (103). We allow for an unknown scale factor in the calculation, as well as a small constant

contribution from the particle-hole excitations. We choose a specific value of the cutoff $\Lambda$, but as noted earlier, the results do not depend strongly on the precise choice. Due to the soft nature of the onset predicted, it is only realistic to compare the initial onset due to the $k$-$\Lambda$ string, as when moving away from this point less relevant operators will begin to contribute. Comparisons between the prediction of the MIM and numerical results are shown in Fig. 16. The agreement is not perfect, but the results are seen to be compatible. As usual the size of the frequency window in which the MIM prediction applies is not known. The theoretical and numerical results of the onset being convex are in stark contrast to the results of Ref. 50, which for the parameters we consider predicts concave power-law behaviour.

## VI. AWAY FROM $q = 0$

One can easily generalise the results here to examine the conductivity at *finite momentum* i.e. consider

$$\chi^J(\omega, q) = -ie^2 \int_0^\infty dt \sum_{l=-L/2}^{L/2-1} e^{i(\omega t - qla_0)} \langle GS|[J_l(t), J_0(0)]|GS\rangle, \tag{109}$$

for $q \neq 0$. The analysis proceeds in an identical manner to identify the quantities $N_{c,s}^{\rm imp}$, $D_{c,s}^{\rm imp}$, as the high-energy impurity simply shifts its momentum. However, in order to find the threshold away from $q \in [(n-1)\pi, (1-n)\pi]$, umklapp processes must be involved. For an arbitrary filling, these will generically be of a very large order, which will suppress the contributions. The dispersion relation is generically no longer a saddle point and therefore in the region where one impurity is involved and one can linearise, power-law behaviour for the onset will be obtained. For the $k$-$\Lambda$ string at momentum $q$, one must first solve for $\Lambda^p$ such that $p_{k\Lambda}(\Lambda^p) = q$, and then $N_c^{\rm imp}(\Lambda^p)$, $D_c^{\rm imp}(\Lambda^p)$ can be calculated. $\gamma$ is still given by (101). The most relevant contribution will then have the form

$$\text{Im } \chi(\omega, q \neq 0) \sim \frac{1}{(\omega - \omega_{\rm th}(q))^{\gamma(\Lambda^p)}}, \tag{110}$$

where $\gamma(\Lambda^p)$ is a function of the quantities $N_\alpha^{\rm imp}$, $D_\alpha^{\rm imp}$ and $K_\alpha$.

## VII. SUMMARY AND CONCLUSIONS

We have studied the optical conductivity $\sigma_1(\omega)$ in the one dimensional Hubbard at zero temperature and close to half filling. Recent DMRG computations[59] have shown that in this regime $\sigma_1(\omega)$ is very small within a "pseudo-gap" and exhibits a rapid increase above an energy scale $E_{\rm opt}$ that depends on doping as well as the interaction strength $U$. Using the Bethe Ansatz we have identified the relevant excitations that contribute to $\sigma_1(\omega)$ for $\omega > E_{\rm opt}$. One of these, the $k$-$\Lambda$ string excitation, had been previously proposed to describe the scale $E_{\rm opt}$[50]. We then followed Ref. 35 to construct a mobile impurity model describing the behaviour of $\sigma_1(\omega)$ above $E_{\rm opt}$. The analysis of this model entailed several generalizations relating to the projection of lattice operators to local fields in the MIM, the treatment of excitations that are not highest weight states with respect to the $\eta$-pairing algebra of the Hubbard model, and considering the mobile impurity to be located at a maximum of its dispersion. We also derived an explicit expression for the finite-size momentum of the relevant Bethe Ansatz states, which is useful in determining the various unknown parameters in the MIM. Our main result is to show that the MIM approach predicts a smooth, slow increase in $\sigma_1(\omega)$ for frequencies above $E_{\rm opt}$. This is in contrast to the half-filled case[40] and previous predictions[50], but consistent with recent dynamical DMRG computations[59]. The results presented in this work are by construction specific to the Hubbard model. However, we expect the gross features seen in the optical conductivity to be quite general for weakly doped Mott insulators. In particular, we expect that such systems to exhibit a rapid increase of $\sigma_1(\omega)$ above a pseudo-gap. As the functional form of the increase is non-universal, it is conceivable that for other models it could be considerably steeper than in the case considered here.

## VIII. ACKNOWLEDGEMENTS

We thank Imke Schneider and Alexander Tiegel for helpful discussions. This work was supported by the EPSRC under grants EP/I032487/1 and EP/J014885/1.

### Appendix A: Velocities and Luttinger parameters in zero magnetic field

In zero magnetic field the charge and spin velocities are given in terms of the solutions to the linear integral equations (32), (33), (36), (37) for the dressed energies and root densities as

$$v_c = \frac{\varepsilon_c'(Q)}{2\pi\rho_{c,0}(Q)}\ , \qquad v_s = \frac{\varepsilon_s'(\infty)}{2\pi\rho_{s,0}(\infty)}. \tag{A1}$$

The spin Luttinger parameter is fixed by spin rotational symmetry to be

$$K_s = 1. \tag{A2}$$

We stress that all spin excitations relevant to our mobile impurity model description occur at (approximately) zero energy, so that corrections to (A2) are negligible. The charge Luttinger parameter is

$$K_c = \frac{\xi^2(Q)}{2}, \tag{A3}$$

where $\xi(k)$ is the solution of the linear integral equation

$$\xi(k) = 1 + \int_{-Q}^{Q} \mathrm{d}k'\ \cos k'\ R(\sin k - \sin k')\ \xi(k'). \tag{A4}$$

Here $R(x)$ is defined in (89).

### Appendix B: Bethe Ansatz results for $k$-$\Lambda$ string

Having established that the threshold above the low-energy continuum can be explained by a $k$-$\Lambda$ string excitation, the simplest equations to consider are the Takahashi equations[2] in the presence of a single $k$-$\Lambda$ string of length 2 i.e. consisting of 1 $\Lambda$ and 2 $k$s. It is also clear that as the correlator is a zero momentum quantity, $k$-$\Lambda$ string is pinned to zero momentum. The Takahashi equations can be analysed for large $L$, keeping terms to $\mathcal{O}(L^{-2})$ in order to calculate the finite-size corrections to the energy. The counting functions in this specific case are given by

$$\begin{aligned} Lz_c(k_j) &= k_j L + \sum_{\alpha=1}^{M-1} \theta\left(\frac{\sin k_j - \Lambda_\alpha}{u}\right) + \theta\left(\frac{\sin k_j - \Lambda'^p}{u}\right), \quad j = 1, \ldots, N-2, \\ Lz_s(\Lambda_\alpha) &= \sum_{j=1}^{N-2} \theta\left(\frac{\Lambda - \sin k_j}{u}\right) - \sum_{\beta=1}^{M-1} \theta\left(\frac{\Lambda_\alpha - \Lambda_\beta}{2u}\right), \qquad \alpha = 1, \ldots, M-1. \end{aligned} \tag{B1}$$

Employing the Euler-Maclaurin summation formula

$$\frac{1}{L}\sum_{n=n_1}^{n_2} f\left(\frac{n}{L}\right) = \int_{\frac{n_-}{L}}^{\frac{n_+}{L}} dx\ f(x) + \frac{1}{24L^2}\left(f'\left(\frac{n_-}{L}\right) - f'\left(\frac{n_+}{L}\right)\right) + \ldots, \tag{B2}$$

where $n_+ = n_2 + \frac{1}{2}$ and $n_- = n_1 - \frac{1}{2}$, it can be seen that

$$\begin{aligned} z_c(k) &= k + \int_{A_-}^{A_+} \mathrm{d}\Lambda\ \theta\left(\frac{\sin k - \Lambda}{u}\right)\rho_s(\Lambda) + \frac{1}{L}\theta\left(\frac{\sin k - \Lambda'^p}{u}\right) \\ &\quad + \frac{2\pi}{24L^2}\left[\frac{a_1(\sin k - A_+)}{\rho_s(A_+)} - \frac{a_1(\sin k - A_-)}{\rho_s(A_-)}\right], \end{aligned} \tag{B3}$$

$$\begin{aligned} z_s(\Lambda) &= \int_{Q_-}^{Q_+} dk\ \theta\left(\frac{\Lambda - \sin k}{u}\right)\rho_c(k) - \int_{A_-}^{A_+} d\Lambda'\ \theta\left(\frac{\Lambda - \Lambda'}{2u}\right)\rho_s(\Lambda') \\ &\quad + \frac{2\pi}{24L^2}\left[\frac{a_1(\Lambda - \sin Q_+)\cos Q_+}{\rho_c(Q_+)} - \frac{a_1(\Lambda - \sin Q_-)\cos Q_-}{\rho_c(Q_+)} - \frac{a_2(\Lambda - A_+)}{\rho_s(A_+)} + \frac{a_2(\Lambda - A_-)}{\rho_s(A_-)}\right]. \end{aligned} \tag{B4}$$

Taking derivatives, equations for the root densities can be found

$$\begin{aligned}\rho_c(k) = \frac{1}{2\pi} + \int_{A_-}^{A_+} d\Lambda\ \cos k\, a_1(\sin k - \Lambda)\rho_s(\Lambda) + \frac{1}{L}\cos k\, a_1(\sin k - \Lambda'^p) \\ + \frac{1}{24L^2}\left[\frac{\cos k\, a_1'(\sin k - A_+)}{\rho_s(A_+)} - \frac{\cos k\, a_1'(\sin k - A_-)}{\rho_s(A_-)}\right],\end{aligned} \tag{B5}$$

$$\begin{aligned}\rho_s(\Lambda) = \int_{Q_-}^{Q_+} dk\ a_1(\Lambda - \sin k)\rho_c(k) - \int_{A_-}^{A_+} d\Lambda'\ a_2(\Lambda - \Lambda')\rho_s(\Lambda') \\ + \frac{1}{24L^2}\left[\frac{a_1'(\Lambda - \sin Q_+)\cos Q_+}{\rho_c(Q_+)} - \frac{a_1'(\Lambda - \sin Q_-)\cos Q_-}{\rho_c(Q_-)} - \frac{a_2'(\Lambda - A_+)}{\rho_s(A_+)} + \frac{a_2'(\Lambda - A_-)}{\rho_s(A_-)}\right].\end{aligned} \tag{B6}$$

As the integral equations are linear, we can write

$$\rho_\alpha(z_\alpha) := \rho_{\alpha,0}(z_\alpha) + \frac{1}{L}\rho_{\alpha,1}(z_\alpha) + \frac{1}{24L^2}\sum_{\beta,\sigma}\frac{f_{\alpha\beta}^{(\sigma)}(z)}{\rho_\beta(X_\sigma^\beta)}, \tag{B7}$$

here $X_\sigma^c = Q_\sigma$, $X_\sigma^s = A_\sigma$. The integral equations satisfied by the first two terms in (B7) are

$$\rho_{\alpha,a}(z) = \rho_{\alpha,a}^{(0)}(z) + K_{\alpha\beta} * \rho_{\beta,a}, \qquad a = 0, 1, \tag{B8}$$

with $K_{\alpha\beta} * f_\beta$ denoting the convolution $\sum_\beta \int_{X_-^\beta}^{X_+^\beta} \mathrm{d}z_\beta\, K_{\alpha\beta}(z_\alpha, z_\beta) f_\beta(z_\beta)$, the kernels defined by

$$\begin{aligned} K_{cc}(k,k') = 0, \qquad & K_{cs}(k,\Lambda) = \cos k\, a_1(\sin k - \Lambda), \\ K_{sc}(\Lambda,k) = a_1(\Lambda - \sin k), \qquad & K_{ss}(\Lambda,\Lambda') = -a_2(\Lambda - \Lambda'), \end{aligned} \tag{B9}$$

and the driving terms given by

$$\rho_{\alpha,0}^{(0)} = \frac{\delta_{\alpha,c}}{2\pi}, \tag{B10}$$

$$\rho_{\alpha,1}^{(0)} = \delta_{\alpha,c}\cos k\ a_1(\sin k - \Lambda'^p). \tag{B11}$$

The final integral equation is determined by

$$f_{\alpha\beta}^{(\sigma)} = d_{\alpha\beta}^{(\sigma)} + K_{\alpha\gamma} * f_{\gamma\beta}^{(\sigma)}, \tag{B12}$$

where

$$d_{\alpha\beta}^{(\sigma)} = -\sigma\frac{\partial}{\partial z'}K_{\alpha\beta}(z,z')\Big|_{z'=X_\sigma^\beta}. \tag{B13}$$

The exact finite-size energy of the system is given by (27). Using the Euler-Maclaurin summation formula (B2) again, corrections can be kept to $\mathcal{O}(L^{-1})$, yielding

$$E = Lu + L\sum_\alpha \int_{X_-^\alpha}^{X_+^\alpha} dz\ \varepsilon_\alpha^{(0)}(z)\rho_\alpha(z) + \varepsilon_{k\Lambda}^{(0)}(\Lambda'^p). \tag{B14}$$

Expanding in powers of $L$ and exploiting the identical kernels of the integral equations for dressed charge and root density equations, if the energy is now considered as a functional of the integration boundaries, performing an expansion about $\sigma X^\alpha$ to second order (the first order term vanishes)[25], it can be shown that

$$E = Le_{GS}(\{X^\alpha\}) + \varepsilon_{k\Lambda}(\Lambda'^p) + L\pi\sum_\alpha v_\alpha\left\{\left(\rho_{\alpha,0}(X^\alpha)(X_+^\alpha - X^\alpha)\right)^2 + \left(\rho_{\alpha,0}(X^\alpha)(X_-^\alpha + X^\alpha)\right)^2\right\} \tag{B15}$$

### 1. Impurity densities

The following are taken as definitions

$$n_\alpha = \int_{X_-^\alpha}^{X_+^\alpha} dz\ \rho_\alpha(z), \tag{B16}$$

$$2D_c = I_+ + I_- = \frac{L}{2\pi}\left[z_c(Q_+) + z_c(Q_-)\right], \tag{B17}$$

$$2D_s = J_+ + J_- = \frac{L}{2\pi}\left[z_s(A_+) + z_s(A_-)\right]. \tag{B18}$$

The corrections from adding the "impurity" i.e. the high-energy excitation can be identified and separated off from the terms that would be present without it. This is achieved by using that

$$\lim_{\Lambda\to\infty} z_s(\Lambda) = -\lim_{\Lambda\to-\infty} z_s(\Lambda), \tag{B19}$$

$$\lim_{k\to\pm\pi} z_c(k) = -\int_{A_-}^{A_+} d\Lambda\ \theta\left(\frac{\Lambda}{u}\right)\rho_s(\Lambda) - \theta\left(\frac{\Lambda'^p}{u}\right). \tag{B20}$$

This allows the "quantum numbers" to be expressed in terms of integrals of the root densities, which can then be split off order-by-order in $1/L$. More explicitly, one finds that

$$\begin{aligned} 2D_s &= L\left(\int_{-\infty}^{A_-} d\Lambda\ \rho_s(\Lambda) - \int_{A_+}^{\infty} d\Lambda\ \rho_s(\Lambda)\right), \\ &= L\left(\int_{-\infty}^{A_-} d\Lambda\ \rho_{s,0}(\Lambda) - \int_{A_+}^{\infty} d\Lambda\ \rho_{s,0}(\Lambda)\right) + 2D_s^{\mathrm{imp}}, \end{aligned} \tag{B21}$$

where

$$2D_s^{\mathrm{imp}} = \int_{-\infty}^{-A} d\Lambda\ \rho_{s,1}(\Lambda) - \int_{A}^{\infty} d\Lambda\ \rho_{s,1}(\Lambda). \tag{B22}$$

Similarly for the charge sector

$$\begin{aligned} 2D_c &= \frac{L}{2\pi}\left(z_c(Q_+) + z_c(Q_-) - z_c(\pi) - z_c(-\pi) - 2\int_{A_-}^{A_+} d\Lambda\ \rho_s(\Lambda)\theta\left(\frac{\Lambda}{u}\right) - \frac{2}{L}\theta\left(\frac{\Lambda'^p}{u}\right)\right), \\ &= L\left(\int_{-\pi}^{Q_-} dk\ \rho_{c,0}(k) - \int_{Q_+}^{\pi} dk\ \rho_{c,0}(k) - \frac{1}{\pi}\int_{A_-}^{A_+} d\Lambda\ \rho_{s,0}(\Lambda)\theta\left(\frac{\Lambda}{u}\right)\right) + 2D_c^{\mathrm{imp}}, \end{aligned} \tag{B23}$$

$$2D_c^{\mathrm{imp}} = \int_{-\pi}^{-Q} dk\ \rho_{c,1}(k) - \int_{Q}^{\pi} dk\ \rho_{c,1}(k) - \frac{1}{\pi}\int_{-A}^{A} d\Lambda\ \rho_{s,1}(\Lambda)\theta\left(\frac{\Lambda}{u}\right) - \frac{1}{\pi}\theta\left(\frac{\Lambda'^p}{u}\right). \tag{B24}$$

Similarly,

$$N_\alpha^{\mathrm{imp}} = \int_{-X^\alpha}^{X^\alpha} dz\ \rho_{\alpha,1}(z). \tag{B25}$$

### 2. Relation between $X_\sigma^\alpha - \sigma X^\alpha$ and the impurity densities

Following Ref. 25, considering the variation of the integration bounds $X_\sigma^\alpha$ with respect to $n_\beta$, it can be seen that, in terms of the dressed charge matrix[2] $Z_{\alpha\beta}$, defined by

$$\begin{aligned} Z_{\alpha\beta} &= \xi_{\alpha\beta}(X^\beta), \\ \xi_{\alpha\beta}(z_\beta) &= \delta_{\alpha\beta} + \xi_{\alpha\gamma} * K_{\gamma\beta}, \end{aligned} \tag{B26}$$

with $K_{\alpha\beta}$ given by (B9), one finds

$$X^{\alpha}_{\sigma} - \sigma X^{\alpha} = \sigma \frac{1}{2} \frac{Z^{-1}_{\alpha\beta}}{\rho_{\alpha,0}(X^{\alpha})} \left( \Delta n_{\beta} - \frac{1}{L} N^{\rm imp}_{\beta} \right) + \frac{Z^{\top}_{\alpha\beta}}{\rho_{\alpha,0}(X^{\alpha})} \left( d_{\beta} - \frac{1}{L} D^{\rm imp}_{\beta} \right). \tag{B27}$$

These results can be inserted into the finite-size energy, which now reads as

$$E = L e_{GS}(\{X^{\alpha}\}) + \varepsilon_{k\Lambda}(0) + \frac{1}{L} \left( -\frac{\pi}{6}(v_s + v_c) + 2\pi \left[ \frac{1}{4} \Delta\widetilde{N}_{\alpha} (Z^{\top})^{-1}_{\alpha\gamma} v_{\gamma} Z^{-1}_{\gamma\beta} \Delta\widetilde{N}_{\beta} + \widetilde{D}_{\alpha} Z_{\alpha\gamma} v_{\gamma} Z^{\top}_{\gamma\beta} \widetilde{D}_{\beta} \right] \right), \tag{B28}$$

where

$$\widetilde{D}_{\alpha} = D_{\alpha} - D^{\rm imp}_{\alpha}, \tag{B29}$$

$$\Delta\widetilde{N}_{\alpha} = \Delta N_{\alpha} - N^{\rm imp}_{\alpha}. \tag{B30}$$

### 3. Simplifications for zero magnetic field

In the $B \to 0$ limit, the integration boundary $A \to \infty$ and many results simplify by use of Fourier transforms. Useful identities used can be found in Ch. 17 of Ref. 2. First, the dressed charge matrix adopts the simple form

$$Z = \begin{pmatrix} \xi & 0 \\ \frac{\xi}{2} & \frac{1}{\sqrt{2}} \end{pmatrix}, \tag{B31}$$

where $\xi = \xi(Q)$ and $\xi(k)$ obeys (A4). Following a similar method to Ref. 25, the root densities can be shown to simplify as

$$\rho_{c,1}(k) = \cos k \; a_1(\sin k - \Lambda'^{p}) + \cos k \int_{-Q}^{Q} dk' \; \rho_{c,1}(k') R(\sin k - \sin k'), \tag{B32}$$

$$\rho_{s,1}(\Lambda) = \int_{-Q}^{Q} dk \; \rho_{c,1}(k) \; s(\Lambda - \sin k), \tag{B33}$$

where

$$s(x) = \frac{1}{4u \cosh\left(\frac{\pi x}{2u}\right)}. \tag{B34}$$

Considering the Fourier transform of (B33), it can be shown that

$$N^{\rm imp}_{s} = \frac{1}{2} N^{\rm imp}_{c}. \tag{B35}$$

In the $\Lambda'^{p} \to 0$ limit, both $\rho_{c,1}(k)$ and $\rho_{s,1}(\Lambda)$ are even functions and therefore

$$D^{\rm imp}_{c} = D^{\rm imp}_{s} = 0. \tag{B36}$$

It is useful to note that the dressed energies take the form

$$\varepsilon_c(k) = -2\cos k - \mu - 2u + \int_{-Q}^{Q} {\rm d}k' \; \cos k' \; R(\sin k - \sin k') \varepsilon_c(k'), \tag{B37}$$

$$\varepsilon_s(\Lambda) = \int_{-Q}^{Q} dk \;\; \cos k \; s\left[\Lambda - \sin k\right] \; \varepsilon_c(k), \tag{B38}$$

$$\varepsilon_{k\Lambda}(\Lambda) = 4{\rm Re}\sqrt{1 - (\Lambda - iu)^2} - 2\mu - 4u + \int_{-Q}^{Q} dk \cos k \; a_1(\sin k - \Lambda) \; \varepsilon_c(k). \tag{B39}$$

The value of $\varepsilon_{k\Lambda}(0)$ provides the location of the threshold at zero momentum in this sector. The finite-size energy can therefore be simply written as

$$E = L e_{GS}(\{X^{\alpha}\}) + \varepsilon_{k\Lambda}(0) - \frac{\pi v_c}{6L} + \frac{2\pi v_c}{L} \left[ \frac{(\Delta N_c - N^{\rm imp}_{c})^2}{4\xi^2} + \xi^2 \left( D_c - D^{\rm imp}_{c} + \frac{D_s - D^{\rm imp}_{s}}{2} \right)^2 \right]. \tag{B40}$$

## Appendix C: Bethe Ansatz results for high-energy charge particle

### 1. Bethe Ansatz calculation

Starting from the Takahashi equations

$$\begin{aligned} Lz_c(k_j) &= k_j L + \sum_{\alpha=1}^{M} \theta\left(\frac{\sin k_j - \Lambda_\alpha}{u}\right), && j = 1, \ldots, N, \\ Lz_s(\Lambda_\alpha) &= \sum_{j=1}^{N} \theta\left(\frac{\Lambda_\alpha - \sin k_j}{u}\right) - \sum_{\beta=1}^{M} \theta\left(\frac{\Lambda_\alpha - \Lambda_\beta}{2u}\right), && \alpha = 1, \ldots, M. \end{aligned} \tag{C1}$$

We can use the Euler-Maclaurin formula (B2) to recast this as

$$z_c(k) = k + \int_{A_-}^{A^+} \mathrm{d}\Lambda\, \theta\left(\frac{\sin k - \Lambda}{u}\right) \rho_s(\Lambda) + \frac{2\pi}{24L^2}\left[\frac{a_1(\sin k - A_+)}{\rho_s(A_+)} - \frac{a_1(\sin k - A_-)}{\rho_s(A_-)}\right], \tag{C2}$$

$$\begin{aligned} z_s(\Lambda) = &\int_{Q_-}^{Q_+} \mathrm{d}k\, \theta\left(\frac{\Lambda - \sin k}{u}\right) \rho_c(k) - \int_{A_-}^{A_+} \mathrm{d}\Lambda' \theta\left(\frac{\Lambda - \Lambda'}{2u}\right) \rho_s(\Lambda') + \frac{1}{L}\theta\left(\frac{\Lambda - \sin k^p}{u}\right) \\ &+ \frac{2\pi}{24L^2}\left[\frac{a_1(\Lambda - \sin Q_+)\cos Q_+}{\rho_c(Q_+)} - \frac{a_1(\Lambda - \sin Q_-)\cos Q_-}{\rho_c(Q_-)} - \frac{a_2(\Lambda - A_+)}{\rho_s(A_+)} + \frac{a_2(\Lambda - A_-)}{\rho_s(A_-)}\right]. \end{aligned} \tag{C3}$$

Taking derivatives gives the root densities

$$\rho_c(k) = \frac{1}{2\pi} + \int_{A_-}^{A_+} \mathrm{d}\Lambda a_1(\sin k - \Lambda)\rho_s(\Lambda)\cos k + \frac{1}{24L^2}\cos k\left[\frac{a_1'(\sin k - A_+)}{\rho_s(A_+)} - \frac{a_1'(\sin k - A_-)}{\rho_s(A_-)}\right], \tag{C4}$$

$$\begin{aligned} \rho_s(\Lambda) = &\int_{Q_-}^{Q_+} \mathrm{d}k a_1(\Lambda - \sin k)\rho_c(k) - \int_{A_-}^{A_+} \mathrm{d}\Lambda' a_2(\Lambda - \Lambda')\rho_s(\Lambda') + \frac{1}{L} a_1(\Lambda - \sin k^p) \\ &+ \frac{1}{24L^2}\left[\frac{a_1'(\Lambda - \sin Q_+)\cos Q_+}{\rho_c(Q_+)} - \frac{a_1'(\Lambda - \sin Q_-)\cos Q_-}{\rho_c(Q_-)} + \frac{a_2'(\Lambda - A_-)}{\rho_s(A_-)} - \frac{a_2'(\Lambda - A_+)}{\rho_s(A_+)}\right]. \end{aligned} \tag{C5}$$

We can again split these linear integral equations into the form (B7), (B8), (B12) where in this case

$$\rho_{\alpha,0}^{(0)} = \frac{\delta_{\alpha,c}}{2\pi}, \qquad \rho_{\alpha,1}^{(0)}(z_\alpha) = \delta_{\alpha,s} a_1(z_\alpha - \sin k^p). \tag{C6}$$

and the integral kernels are again given by (B9). We can then construct the impurity densities

$$N_\alpha^{\mathrm{imp}} = \int_{-X_\alpha}^{X^\alpha} \mathrm{d}z_\alpha \rho_{\alpha,1}(z_\alpha), \tag{C7}$$

$$2D_c^{\mathrm{imp}} = \int_Q^\pi \mathrm{d}k\, [\rho_{c,1}(-k) - \rho_{c,1}(k)] - \frac{1}{\pi}\int_{-A}^{A} \mathrm{d}\Lambda\, \rho_{s,1}(\Lambda)\, \theta\left(\frac{\Lambda}{u}\right), \tag{C8}$$

$$2D_s^{\mathrm{imp}} = \int_A^\infty \mathrm{d}\Lambda\, [\rho_{s,1}(-\Lambda) - \rho_{s,1}(\Lambda)]. \tag{C9}$$

To determine the thermodynamic rapidity $k^p$ and the finite-size correction $\delta k^p$, we can examine the requirements that

$$z_c(k_L^p) = \frac{2\pi I^p}{L}, \tag{C10}$$

$$z_{c,0}(k^p) = \frac{2\pi I^p}{L}, \tag{C11}$$

with $k_L^p = k^p + \frac{\delta k^p}{L}$. Expanding (C10) in the deviation $\delta k^p$ and using (C11) yields

$$\delta k^p = -\frac{L}{2\pi\rho_{c,0}(k^p)}\left[\sum_{\beta,\sigma} \Psi_\beta^{(\sigma)}(k^p)(X_\beta^\sigma - \sigma X^\beta)\right] - \frac{1}{2\pi\rho_{c,0}(k^p)}\int_{-A}^{A} \mathrm{d}\Lambda \rho_{s,1}(\Lambda)\theta\left(\frac{\Lambda - \sin k^p}{u}\right), \tag{C12}$$

where

$$\Psi_\beta^{(\sigma)}(k) = \sigma\rho_{s,0}(A)\theta\left(\frac{\sigma A - \sin k}{u}\right)\delta_{s,\beta} + \int_{-A}^{A} \mathrm{d}\Lambda\, r_{s,\beta}^{(\sigma)}(\Lambda)\theta\left(\frac{\Lambda - \sin k}{u}\right), \tag{C13}$$

$$r_{\alpha\beta}^{(\sigma)} = \sigma\rho_{\beta,0}(X^\beta)K_{\alpha\beta}(z_\alpha, \sigma X^\beta) + K_{\alpha\gamma} * r_{\gamma\beta}^{(\sigma)}. \tag{C14}$$

Using the results of Appendix E, this can be shown to reduce to

$$\delta k^p = \frac{1}{\rho_{c,0}(k^p)} \sum_{\alpha=c,s} \left(N_\alpha^{\mathrm{imp}} D_\alpha + D_\alpha^{\mathrm{imp}} \Delta N_\alpha - D_\alpha^{\mathrm{imp}} N_\alpha^{\mathrm{imp}}\right). \tag{C15}$$

We then have that

$$E = e_{GS}L + \varepsilon_c(k^p) + \varepsilon_c'(k^p)\frac{\delta k^p}{L} - \frac{\pi}{6L}(v_s + v_c) + \frac{2\pi}{L}\left[\frac{1}{4}\Delta\widetilde{N}_\gamma (Z^\top)^{-1}_{\gamma\alpha} v_\alpha Z^{-1}_{\alpha\beta}\Delta\widetilde{N}_\beta + \widetilde{D}_\gamma Z_{\gamma\alpha} v_\alpha Z^\top_{\alpha\beta}\widetilde{D}_\beta\right], \tag{C16}$$

with the form of $\widetilde{D}_\alpha$, $\Delta\widetilde{N}_\alpha$ and $Z_{\alpha\beta}$ given by (B29), (B30), (B26).

### 2. Simplification for $B \to 0$

In the $B \to 0$ limit, the integral equations describing the impurity densities are given by

$$\rho_{c,1}(k) = \cos k\, R(\sin k - \sin k^p) + \cos k \int_{-Q}^{Q} \mathrm{d}k'\, R(\sin k - \sin k')\rho_{c,1}(k'), \tag{C17}$$

$$N_c^{\mathrm{imp}} = \int_{-Q}^{Q} \mathrm{d}k \rho_{c,1}(k), \qquad N_s^{\mathrm{imp}} = \frac{1}{2}(1 + N_c^{\mathrm{imp}}), \tag{C18}$$

$$\begin{aligned} 2D_c^{\mathrm{imp}} = &\int_Q^\pi \mathrm{d}k\left[\rho_{c,1}(-k) - \rho_{c,1}(k)\right] + \frac{i}{\pi}\left\{\ln\left[\frac{\Gamma\left(\frac{1}{2} - i\frac{\sin k^p}{4u}\right)\Gamma\left(1 + i\frac{\sin k^p}{4u}\right)}{\Gamma\left(\frac{1}{2} + i\frac{\sin k^p}{4u}\right)\Gamma\left(1 - i\frac{\sin k^p}{4u}\right)}\right]\right\} \\ &+ \frac{i}{\pi}\int_{-Q}^{Q} \mathrm{d}k \rho_{c,1}(k)\left\{\ln\left[\frac{\Gamma\left(\frac{1}{2} - i\frac{\sin k}{4u}\right)\Gamma\left(1 + i\frac{\sin k}{4u}\right)}{\Gamma\left(\frac{1}{2} + i\frac{\sin k}{4u}\right)\Gamma\left(1 - i\frac{\sin k}{4u}\right)}\right]\right\}, \end{aligned} \tag{C19}$$

$$D_s^{\mathrm{imp}} = 0. \tag{C20}$$

This gives the finite-size corrections to the energy as

$$\begin{aligned} E = &e_{GS}L + \varepsilon_c(k^p) + \varepsilon'(k^p)\frac{\delta k^p}{L} - \frac{\pi v_c}{6L} \\ &+ \frac{2\pi v_c}{L}\left[\frac{(\Delta N_c - N_c^{\mathrm{imp}})^2}{4\xi^2} + \xi^2\left(D_c - D_c^{\mathrm{imp}} + \frac{D_s}{2}\right)^2\right] \\ &+ \frac{2\pi v_s}{L}\left[\frac{1}{2}\left(\Delta N_s - \frac{\Delta N_c}{2} - \frac{1}{2}\right)^2 + \frac{D_s^2}{2}\right], \end{aligned} \tag{C21}$$

where $\xi = \xi(Q)$ and $\xi(k)$ obeys (A4).

## Appendix D: Bethe Ansatz results for two high-energy charge hole excitations

We again start from (C1). Following similar steps to Appendices B and C, applying the Euler-Maclaurin summation formula (B2) then allows us to write

$$\rho_\alpha(z_\alpha) = \rho_{\alpha,0}(z_\alpha) + \frac{1}{L}\rho_{\alpha,1}(z_\alpha) + \frac{1}{24L^2}\sum_{\beta,\sigma}\frac{f_{\alpha\beta}^{(\sigma)}(z_\alpha)}{\rho_\beta(X_\sigma^\beta)}. \tag{D1}$$

We can again split these linear integral equations into the form (B7), (B8), (B12) where in this case

$$\rho^{(0)}_{\alpha,0} = \frac{\delta_{\alpha,c}}{2\pi}, \tag{D2}$$

$$\rho^{(0)}_{\alpha,1} = -\delta_{\alpha,s}\left[a_1(\Lambda - \sin k^{h_1}) + a_1(\Lambda - \sin k^{h_2})\right]. \tag{D3}$$

and the integral kernels are given by (B9). We can now determine

$$2D_c^{\rm imp} = \int_Q^\pi \mathrm{d}k\,[\rho_{c,1}(-k) - \rho_{c,1}(k)] - \frac{1}{\pi}\int_{-A}^{A}\mathrm{d}\Lambda\,\theta\left(\frac{\Lambda}{u}\right)\rho_{s,1}(\Lambda), \tag{D4}$$

$$2D_s^{\rm imp} = \int_A^\infty \mathrm{d}\Lambda\,\left[\rho_{s,1}(-\Lambda) - \rho_{s,1}(\Lambda)\right]. \tag{D5}$$

We also have that

$$z_c(k_L^{h_i}) = \frac{2\pi I^{h_i}}{L}, \qquad z_{c,0}(k^{h_i}) = \frac{2\pi I^{h_i}}{L}, \tag{D6}$$

with $k_L^{h_i} = k^{h_i} + \frac{\delta k^{h_i}}{L}$, yielding

$$\delta k^{h_i} = -\frac{L}{2\pi\rho_{c,0}(k^{h_i})}\left[\sum_{\beta,\sigma}\Psi_\beta^{(\sigma)}(k^{h_i})(X_\beta^\sigma - \sigma X^\beta)\right] - \frac{1}{2\pi\rho_{c,0}(k^{h_i})}\int_{-A}^{A}\mathrm{d}\Lambda\rho_{s,1}(\Lambda)\theta\left(\frac{\Lambda - \sin k^{h_i}}{u}\right), \tag{D7}$$

with $\Psi^{(\sigma)}(k)$ given by (C13). We now have all of the quantities required to evaluate the finite-size spectrum in the presence of the two high-energy holons:

$$\begin{aligned} E = {} & e_{GS}L - \varepsilon_c(k^{h_1}) - \varepsilon_c(k^{h_2}) - \varepsilon_c'(k^{h_1})\frac{\delta k^{h_1}}{L} - \varepsilon_c'(k^{h_2})\frac{\delta k^{h_2}}{L} - \frac{\pi}{6L}(v_s + v_c) \\ & + \frac{2\pi}{L}\left[\frac{1}{4}\Delta\widetilde{N}_\gamma(Z^\top)^{-1}_{\gamma\alpha}v_\alpha Z^{-1}_{\alpha\beta}\Delta\widetilde{N}_\beta + \widetilde{D}_\gamma Z_{\gamma\alpha}v_\alpha Z^\top_{\alpha\beta}\widetilde{D}_\beta\right], \end{aligned} \tag{D8}$$

with the form of $\widetilde{D}_\alpha$, $\Delta\widetilde{N}_\alpha$ and $Z_{\alpha\beta}$ given by (B29), (B30), (B26).

### 1. Zero field

In zero field, the integral equations for the functions $\rho_{c,1}$, $\rho_{s,1}$ simplify due to $A \to \infty$ allowing the use of a Fourier transform, specifically

$$\rho_{c,1}(k) = -\cos k\left[R(\sin k - \sin k^{h_1}) + R(\sin k - \sin k^{h_2})\right] + \cos k\int_{-Q}^{Q}\mathrm{d}k'\,R(\sin k - \sin k')\rho_{c,1}(k'), \tag{D9}$$

$$\rho_{s,1} = -s(\Lambda - \sin k^{h_1}) - s(\Lambda - \sin k^{h_2}) + \int_{-Q}^{Q}\mathrm{d}k\,s(\Lambda - \sin k)\rho_{c,1}(k). \tag{D10}$$

We also have

$$N_s^{\rm imp} = \frac{1}{2}N_c^{\rm imp} - 1. \tag{D11}$$

The finite-size spectrum can then be written as

$$\begin{aligned} E = {} & e_{GS}L - \varepsilon_c(k^{h_1}) - \varepsilon_c(k^{h_2}) - \frac{\delta k^{h_1}}{L}\varepsilon_c'(k^{h_1}) - \frac{\delta k^{h_2}}{L}\varepsilon_c'(k^{h_2}) - \frac{\pi}{6L}(v_c + v_s) \\ & + \frac{2\pi v_c}{L}\left[\frac{(\Delta N_c - N_c^{\rm imp})^2}{4\xi^2} + \xi^2\left(D_c - D_c^{\rm imp} + \frac{D_s - D_s^{\rm imp}}{2}\right)^2\right] \\ & + \frac{2\pi v_s}{L}\left[\frac{1}{2}\left(\Delta N_s - \frac{\Delta N_c}{2} + 1\right)^2 + \frac{(D_s - D_s^{\rm imp})^2}{2}\right]. \end{aligned} \tag{D12}$$

## Appendix E: Finite-size momentum spectrum

As well as the finite-size energies, it is also possible to match the finite-size momentum spectra. We consider here the simple case of a single high-energy charge excitation, but the reasoning is the same for other excitations.

### 1. Mobile impurity model momentum spectrum

We bosonise the Hubbard chain at $U = 0$, decomposing the fermionic annihilation operator as

$$c_\sigma(x) = R_\sigma(x)e^{ik_F x} + L_\sigma(x)e^{-ik_F x}. \tag{E1}$$

To identify the momentum operator, we consider it as the generator of translations by one site i.e.

$$e^{-ia_0 P}c_\sigma(x)e^{ia_0 P} = c_\sigma(x + a_0). \tag{E2}$$

Which means that $R_\sigma(x) \to R_\sigma(x + a_0)e^{ik_F a_0}$. By utilising the refermionisation identities[35]

$$R_\uparrow \sim \prod_{\alpha=c,s} e^{-\frac{i}{\sqrt{2}}\varphi^*_\alpha + \frac{i}{4\sqrt{2}}\Phi^*_\alpha}, \qquad L_\uparrow \sim \prod_{\alpha=c,s} e^{\frac{i}{\sqrt{2}}\bar{\varphi}^*_\alpha - \frac{i}{4\sqrt{2}}\Phi^*_\alpha}, \tag{E3}$$

we can identify that, in terms of the mode expansion of the spin and charge modes, the momentum operator is given by

$$\begin{aligned} P = &\frac{k_F}{\pi\sqrt{2}}\left(\bar{Q}^*_c - Q^*_c\right) + \frac{1}{8\pi L}\left[Q^{*2}_c - \bar{Q}^{*2}_c + Q^{*2}_s - \bar{Q}^{*2}_s\right] \\ &+ i\int \mathrm{d}x B^\dagger(x)\partial_x B(x) + \sum_{\alpha=c,s}\sum_{n=1}^{\infty}\frac{2\pi n}{L}\left(c^\dagger_{\alpha,R,n}c_{\alpha,R,n} - c^\dagger_{\alpha,L,n}c_{\alpha,L,n}\right). \end{aligned} \tag{E4}$$

Employing the unitary transformation, this can be written as

$$\begin{aligned} P = &\frac{k_F}{\pi\sqrt{2}}\left(\bar{Q}^\circ_c - \bar{Q}^\circ_c - 4\pi\gamma_c + 4\pi\bar{\gamma}_c\right) + \frac{1}{8\pi L}\left[Q^{\circ 2}_c - \bar{Q}^{\circ 2}_c + Q^{\circ 2}_s - \bar{Q}^{\circ 2}_s\right] + i\int \mathrm{d}x \widetilde{B}^\dagger\partial_x\widetilde{B} \\ &+ \sum_{\alpha=c,s}\sum_{n=1}^{\infty}\frac{2\pi n}{L}\left(c^\dagger_{\alpha,R,n}c_{\alpha,R,n} - c^\dagger_{\alpha,L,n}c_{\alpha,L,n}\right). \end{aligned} \tag{E5}$$

Which therefore predicts a finite-size spectrum of the form

$$\begin{aligned} P = &\frac{k_F}{\pi\sqrt{2}}\left(\bar{q}_c - q_c\right) + P_{mimp}(k^p) + \frac{2\pi}{L}\left[\left(\frac{q_c + \bar{q}_c}{4\pi} - \gamma_c + \bar{\gamma}_c\right)\left(\frac{q_c - \bar{q}_c}{4\pi} - \gamma_c - \bar{\gamma}_c\right) + \right. \\ &\left.\left(\frac{q_s + \bar{q}_s}{4\pi} - \gamma_s + \bar{\gamma}_s\right)\left(\frac{q_s - \bar{q}_s}{4\pi} - \gamma_s - \bar{\gamma}_s\right)\right] + \frac{2\pi}{L}\sum_{k=c,s}\left(N^+_k - N^-_k\right), \end{aligned} \tag{E6}$$

where the $N^\pm_k$ are non-negative integers enumerating the number of particle-hole pairs in the vicinity of the "Fermi points".

### 2. Bethe Ansatz calculation: high-energy charge particle

We wish to know the momentum contribution from the high-energy charge particle: there will be finite-size contributions to this from interactions with the low-energy sector. As we know precisely the integers forming this state from (50), we can simply sum these integers to find the momentum. This approach, however, yields no information on which contributions come from the finite-size shift of the rapidity and which contributions come from interactions between the high-energy and low-energy degrees of freedom. The solution is to explicitly include the finite-size shift of the rapidity and calculate the remaining corrections in terms of the quantites $N^{\mathrm{imp}}_\alpha$, $D^{\mathrm{imp}}_\alpha$, $N_\alpha$, $D_\alpha$, as we had for the finite-size energy.

*a. Basic integral equations*

The solution for $\rho_{\alpha,1}$ implicitly defined by (C6), can be formally written as

$$\rho_{\alpha,1}(z_\alpha) = \left(K_{\alpha\beta} * (1-\hat{K})^{-1}_{\beta c}\right)(z_\alpha, k^p). \tag{E7}$$

We introduce the shift functions[58]

$$\begin{aligned} F^{(0)}_{cc}(k,k') = 0, \qquad F^{(0)}_{cs}(k,\Lambda) = \frac{1}{2\pi}\theta\left(\frac{\sin k - \Lambda}{u}\right), \\ F^{(0)}_{sc}(\Lambda,k) = \frac{1}{2\pi}\theta\left(\frac{\Lambda - \sin k}{u}\right), \qquad F_{ss}(\Lambda,\Lambda') = -\frac{1}{2\pi}\theta\left(\frac{\Lambda-\Lambda'}{2u}\right), \end{aligned} \tag{E8}$$

and the "dressed" shift functions

$$F_{\alpha\beta}(z_\alpha, z_\beta) = F^{(0)}_{\alpha\beta}(z_\alpha, z_\beta) + \left(F_{\alpha\gamma} * K_{\gamma\beta}\right)(z_\alpha, z_\beta). \tag{E9}$$

It is useful to note that

$$K_{\alpha\beta}(z_\alpha, z_\beta) = \partial_{z_\alpha} F^{(0)}_{\alpha\beta}. \tag{E10}$$

Both the finite-size energy and momentum spectra involve the function

$$\tilde{r}^{(\sigma)}_{\alpha\beta}(z_\alpha) = K_{\alpha\beta}(z_\alpha, \sigma X^\beta) + K_{\alpha\gamma} * \tilde{r}^{(\sigma)}_{\gamma\beta}. \tag{E11}$$

*b. Finite-size momentum spectrum*

As for the energy of the system, the momentum can also be expanded as an asymptotic series in powers of $L^{-1}$. In the analysis of the finite-size energy calculation, when determining $\delta k^p$ as in (C12), one finds

$$\begin{aligned} z_c(k^p_L) = z_{c,0}(k^p) + z'_{c,0}(k^p)\frac{\delta k^p}{L} \\ + \sum_{\sigma,\beta} \sigma\rho_{\beta,0}(X^\beta)\left[\theta\left(\frac{\sin k^p - \sigma X^\beta}{u}\right)\delta_{\beta,s} + \int_{-A}^{A} \mathrm{d}\Lambda\, \theta\left(\frac{\sin k^p - \Lambda}{u}\right)\tilde{r}^{(\sigma)}_{s\beta}(\Lambda)\right]\left[X^\beta_\sigma - \sigma X^\beta\right] \\ + \frac{1}{L}\int_{-A}^{A} \mathrm{d}\Lambda\, \theta\left(\frac{\sin k^p - \Lambda}{u}\right)\rho_{s,1}(\Lambda). \end{aligned} \tag{E12}$$

We will first look at the term in the sum multiplied by $X^\beta_\sigma - \sigma X^\beta$. (E9) and (E11) imply that

$$F_{\alpha\beta} = F^{(0)}_{\alpha\gamma} * (1-\hat{K})^{-1}_{\gamma\beta}, \qquad \tilde{r}^{(\sigma)}_{\alpha\beta} = (1-\hat{K})^{-1}_{\alpha\gamma} * K_{\gamma\beta}(z_\alpha, \sigma X^\beta), \tag{E13}$$

allowing us to write

$$F^{(0)}_{c\beta}(k^p, \sigma X^\beta) + F^{(0)}_{c\alpha} * \tilde{r}^{(\sigma)}_{\alpha\beta}(k^p) = F_{c\beta}(k^p, \sigma X^\beta). \tag{E14}$$

It can also be shown that

$$\int_{-A}^{A} \mathrm{d}\Lambda\, \theta\left(\frac{\sin k - \Lambda}{u}\right)\rho_{s,1}(\Lambda) = 2\pi F_{cc}(k, k^p). \tag{E15}$$

The finite-size momentum can therefore be written in terms of the dressed shift functions as

$$z_c(k^p_L) = z_{c_0}(k^p) + z'_{c,0}(k^p)\frac{\delta k^p}{L} + \sum_{\sigma,\beta} \sigma 2\pi\rho_{\beta,0}(X^\beta)F_{c\beta}(k^p, \sigma X^\beta)\left[X^\beta_\sigma - \sigma X^\beta\right] + \frac{2\pi}{L}F_{cc}(k^p, k^p). \tag{E16}$$

We now wish to relate the functions $F_{\alpha\beta}(z_\alpha, z_\beta)$ to the impurity densities $N^{\mathrm{imp}}_\alpha$, $D^{\mathrm{imp}}_\alpha$.

### c. Relating shift functions to impurity densities

By using (E7) and (E10) in (C7) and (C8), it can be shown that

$$2D_\alpha^{\text{imp}} = F_{\alpha c}(X^\alpha, k^p) + F_{\alpha c}(-X^\alpha, k^p), \tag{E17}$$

$$N_\alpha^{\text{imp}} = F_{\alpha c}(X^\alpha, k^p) - F_{\alpha c}(-X_\alpha, k^p), \tag{E18}$$

i.e.

$$D_\alpha^{\text{imp}} \pm \frac{N_\alpha^{\text{imp}}}{2} = F_{\alpha c}(\pm X^\alpha, k^p). \tag{E19}$$

### d. Determining boundary terms

To express the finite-size momentum (E16) in terms of the $N_\alpha^{\text{imp}}$, $D_\alpha^{\text{imp}}$ (E19), we need to relate $F_{\alpha c}(\sigma X^\alpha, k^p)$ to $F_{c\beta}(k^p, \sigma' X^\beta)$. By considering the Neumann series of (E13) and integrating by parts, it can be shown that

$$F_{\alpha\beta}(z_\alpha, z_\beta) + F_{\beta\alpha}(z_\beta, z_\alpha) = -\sum_{\gamma,\sigma} \sigma F_{\gamma\alpha}(\sigma X^\gamma, z_\alpha) F_{\gamma\beta}(\sigma X^\gamma, z_\beta). \tag{E20}$$

To establish the desired relationship, (E20) implies that we require the values $F_{\alpha\beta}(\tau X^\alpha, \tau' X^\beta)$. It is simple to show that

$$F_{\alpha\beta}(X^\alpha, X^\beta) - F_{\alpha\beta}(-X^\alpha, X^\beta) = Z_{\alpha\beta} - \delta_{\alpha\beta}, \tag{E21}$$

with $Z$ the dressed charge matrix as defined in (B26). (E20) also implies that

$$F_{\alpha\beta}(X^\alpha, X^\beta) + F_{\beta\alpha}(X^\beta, X^\alpha) = -\sum_{\gamma} \left[ F_{\gamma\alpha}(X^\gamma, X^\alpha) F_{\gamma\beta}(X^\gamma, X^\beta) - F_{\gamma\alpha}(-X^\gamma, X^\alpha) F_{\gamma\beta}(-X^\gamma, X^\beta) \right]. \tag{E22}$$

Substituting (E21) into (E22) and simplifying, if we define $F$ to be the matrix $F_{\alpha\beta}(X^\alpha, X^\beta)$, then it satisfies the equation

$$Z^\top F + F^\top Z = (1 - Z)^\top (1 - Z). \tag{E23}$$

Considering

$$F_{\beta\alpha}(-X^\beta, X^\alpha) - F_{\alpha\beta}(-X^\alpha, X^\beta) = \sum_{\sigma,\gamma} \sigma F_{\gamma\alpha}(\sigma X^\gamma, X^\alpha) F_{\gamma\beta}(-\sigma X^\gamma, X^\beta), \tag{E24}$$

and using (E21) again, we find the similar equation

$$Z^\top F - F^\top Z = Z - Z^\top. \tag{E25}$$

(E23) and (E25) determine $F$ uniquely, giving

$$F_{\alpha\beta}(\tau X^\alpha, \tau' X^\beta) = \frac{\tau}{2} (Z - 1)_{\alpha\beta} + \frac{\tau'}{2} \left( Z^{-1^\top} - 1 \right)_{\alpha\beta}. \tag{E26}$$

This therefore allows us to write down the dressed shift functions appearing in (E16) in terms of the known quantities $N_\alpha^{\text{imp}}$, $D_\alpha^{\text{imp}}$, viz.

$$F_{cc}(k^p, k^p) = -\sum_{\gamma} D_\gamma^{\text{imp}} N_\gamma^{\text{imp}}, \tag{E27}$$

$$F_{c\alpha}(k^p, \tau X^\alpha) = -\sum_{\gamma} \left( \frac{\tau}{2} N_\gamma^{\text{imp}} Z^{-1^\top}{}_{\gamma\alpha} + D_\gamma^{\text{imp}} Z_{\gamma\alpha} \right). \tag{E28}$$

Combining the previous results, we find

$$z_c(k_L^p) = z_{c,0}(k^p) + z'_{c,0}(k^p) \frac{\delta k^p}{L} - \frac{2\pi}{L} \sum_{\alpha} \left[ N_\alpha^{\text{imp}} D_\alpha + D_\alpha^{\text{imp}} \Delta N_\alpha - D_\alpha^{\text{imp}} N_\alpha^{\text{imp}} \right]. \tag{E29}$$

Using Eq. (8.38) from Ref. 2, the full finite-size momentum spectrum in the presence of a high-energy charge particle is given by

$$P = 2D_c k_{F,\uparrow} + 2(D_c + D_s)k_{F,\downarrow} + z_{c,0}(k^p) + 2\pi\rho_{c,0}(k^p)\frac{\delta k^p}{L} + \frac{2\pi}{L}\left(\Delta\widetilde{\mathbf{N}}^\top \cdot \Delta\widetilde{\mathbf{D}} + \sum_{k\in\{c,s\}}(N_k^+ - N_k^-)\right), \tag{E30}$$

where the $N_k^\pm$ are non-negative integers enumerating the number of particle-hole pairs in the vicinity of the Fermi points and $k_{F,\uparrow(\downarrow)} = \frac{1}{2}(\pi n_c \pm 2\pi m)$. In the zero-field limit $m = 0$ and therefore $k_{F,\uparrow} = k_{F,\downarrow} = k_F$, giving

$$P = 2k_F(2D_c + D_s) + z_{c,0}(k^p) + 2\pi\rho_{c,0}(k^p)\frac{\delta k^p}{L} + \frac{2\pi}{L}\left(\Delta\widetilde{\mathbf{N}}^\top \cdot \Delta\widetilde{\mathbf{D}} + \sum_{k\in\{c,s\}}(N_k^+ - N_k^-)\right). \tag{E31}$$

## Appendix F: Mobile impurity contributions to $\sigma^{(2)}(\omega)$

### 1. Threshold of the "particle-hole" continuum in $\sigma^{(2)}(\omega)$

Next we examine the thresholds in the second contribution (19) to the optical conductivity. The lowest threshold arises in the "particle-hole" and "two-particle" excitations considered in III C 1 and III C 2 respectively. The threshold in both cases is given by

$$\begin{aligned} E^{\mathrm{ph}}_{\mathrm{thres}}(q) &= \varepsilon_c(k(q)) - 2\mu, \\ q &= k + \int_{-\infty}^{\infty} \mathrm{d}\Lambda\, \theta\left(\frac{\sin k - \Lambda}{u}\right)\rho_{s,0}(\Lambda), \end{aligned} \tag{F1}$$

where $\rho_{s,0}(\Lambda)$ is the ground state root density (33). The threshold for the particle-hole (two-particle) excitation is obtained by fixing the position of the hole (one of the particles) in momentum space at one of the "Fermi points", so that it contributes only at $\mathcal{O}(L^{-1})$ to the excitation energy. Hence the impurity degree of freedom corresponds to a particle in both cases.

#### *a. Projection of the operator $\mathcal{O}_j$*

We will use the representation (18) to determine the contribution $C^{(2)}_{\mathrm{JJ}}(\ell, t)$ to the current-current correlator. Hence we require the projection of the operator $\mathcal{O}_j$ defined in (17) to the mobile impurity model (61). This can be worked out by following Ref. 35. We start by taking the continuum limit of the lattice fermion operators

$$c_{j,\sigma} \sim R_\sigma(x)e^{ik_F x} + L_\sigma(x)e^{-ik_F x} + \dots, \quad x = ja_0 \tag{F2}$$

where $a_0$ is the lattice spacing. The continuum limit of $\mathcal{O}_j$ then takes the form

$$\mathcal{O}(x) \sim e^{ix(2k_F - \pi)}R_c\partial_x R_c e^{i\pi\int_{-\infty}^{x}\mathrm{d}x'\,Q_c(x')} + \dots, \tag{F3}$$

with $Q_c(x) = R_c^\dagger(x)R_c(x) + L_c^\dagger(x)L_c(x)$. Next we decompose the charge part into the low-energy and impurity pieces

$$R_c(x) \sim r_c + B^\dagger(x)e^{i(\pi - 2k_F)x} + \dots. \tag{F4}$$

Substituting this back into (F3) and then bosonising the low-energy degrees of freedom we obtain

$$\mathcal{O}(x) \sim B^\dagger(x)e^{-\frac{i}{2\sqrt{2}}\Theta_c^*(x)} + \dots, \tag{F5}$$

where we have retained only the most relevant piece in the sector with a single impurity.

*b. Finite-size excitation energy in the Mobile Impurity Model*

As the mobile impurity model is again given by (59) to (61), and the impurity again is located at a maximum of its dispersion, we can follow through the same steps as in our analysis of the $k$-$\Lambda$ string threshold. The finite-size spectrum is, accordingly, of the same form as (82). The values of $q_\alpha^{(0)}$ follow from the form of the Luttinger liquid part of (F5) to be

$$q_c^{(0)} = \bar{q}_c^{(0)} = \pi\sqrt{2}; \qquad q_s^{(0)} = \bar{q}_s^{(0)} = 0. \tag{F6}$$

*c. Finite-size excitation energy from Bethe Ansatz*

We consider again the excitation described in Section III C 1. The finite-size corrections to the excitation energy are calculated in Appendix C. The final result is of the form

$$\begin{aligned} E = {} & e_{GS}L + \varepsilon_c(k^p) + \frac{\delta k^p}{L}\varepsilon_c'(k^p) - \frac{\pi}{6L}(v_c + v_s) \\ & + \frac{2\pi v_c}{L}\left[\frac{(\Delta N_c - N_c^{\mathrm{imp}})^2}{8K_c} + 2K_c\left(D_c - D_c^{\mathrm{imp}} + \frac{D_s - D_s^{\mathrm{imp}}}{2}\right)^2\right] \\ & + \frac{2\pi v_s}{L}\left[\frac{1}{2}\left(\Delta N_s - N_s^{\mathrm{imp}} - \frac{\Delta N_c - N_c^{\mathrm{imp}}}{2}\right)^2 + \frac{(D_s - D_s^{\mathrm{imp}})^2}{2}\right]. \end{aligned} \tag{F7}$$

Here the ground state energy per site $e_{GS}$ and dressed energy $\varepsilon_c(k)$ are given in (35) and (36) respectively, while the velocities $v_{s,c}$ and the Luttinger parameter $K_c$ are calculated in Appendix A. The thermodynamic value $k^p$ of the impurity rapidity and its finite-size correction $\delta k^p$ are determined by (C11) and (C15). Finally, we have

$$\begin{aligned} & \Delta N_c = -3\ , \qquad \Delta N_s = -1\ , \qquad D_c = 0\ , \qquad D_s = 0\ , \\ & N_c^{\mathrm{imp}} = 2N_s^{\mathrm{imp}} - 1 = \int_{-Q}^{Q} \mathrm{d}k\, \rho_{c,1}(k)\ , \qquad D_s^{\mathrm{imp}} = 0, \end{aligned} \tag{F8}$$

$$\begin{aligned} 2D_c^{\mathrm{imp}} = {} & \int_Q^\pi \mathrm{d}k\, [\rho_{c,1}(-k) - \rho_{c,1}(k)] + \frac{i}{\pi}\left\{\ln\left[\frac{\Gamma\left(\frac{1}{2} - i\frac{\sin k^p}{4u}\right)\Gamma\left(1 + i\frac{\sin k^p}{4u}\right)}{\Gamma\left(\frac{1}{2} + i\frac{\sin k^p}{4u}\right)\Gamma\left(1 - i\frac{\sin k^p}{4u}\right)}\right]\right\} \\ & + \frac{i}{\pi}\int_{-Q}^{Q} \mathrm{d}k\, \rho_{c,1}(k)\left\{\ln\left[\frac{\Gamma\left(\frac{1}{2} - i\frac{\sin k}{4u}\right)\Gamma\left(1 + i\frac{\sin k}{4u}\right)}{\Gamma\left(\frac{1}{2} + i\frac{\sin k}{4u}\right)\Gamma\left(1 - i\frac{\sin k}{4u}\right)}\right]\right\}, \end{aligned} \tag{F9}$$

where $\rho_{c,1}(k)$ is the solution of the integral equation

$$\rho_{c,1}(k) = \cos k\, R(\sin k - \sin k^p) + \cos k \int_{-Q}^{Q} \mathrm{d}k'\, R(\sin k - \sin k')\rho_{c,1}(k'). \tag{F10}$$

In order to fully specify our mobile impurity model we also require the the curvature of the dispersion relations of $\varepsilon_c(k)$ at $k = \pi$, which is given by

$$-\frac{1}{m} = \left.\frac{\mathrm{d}^2\varepsilon_c(k(q))}{\mathrm{d}q^2}\right|_{k=\pi} = \frac{2 + \int_{-Q}^{Q} \mathrm{d}k\, R'(\sin k)\varepsilon_c'(k)}{(2\pi\rho_{c,0}(\pi))^2}. \tag{F11}$$

*d. Fixing the parameters $\gamma_\alpha$, $\bar{\gamma}_\alpha$*

By matching the expressions (F7) and (82) for the finite-size energies we can fix the parameters $\gamma_\alpha$, $\bar{\gamma}_\alpha$

$$\begin{aligned} & \gamma_c = \frac{1}{2\sqrt{2}} + \frac{1}{2\sqrt{2}}(\Delta N_c - N_c^{\mathrm{imp}})\ , \qquad \gamma_s = 0\ , \\ & \bar{\gamma}_c = -\frac{1}{2\sqrt{2}} - \frac{1}{2\sqrt{2}}(\Delta N_c - N_c^{\mathrm{imp}})\ , \qquad \bar{\gamma}_s = 0. \end{aligned} \tag{F12}$$

### e. *Current-current correlator in the mobile impurity model*

Given the expression (F5) for the projection of the operator $\mathcal{O}_j$, we have

$$C^{(2)}_{\rm JJ}(\ell,t) \sim H(x,t) = \langle \mathcal{O}^\dagger(x,t)\mathcal{O}(0,0)\rangle \sim \langle B(x,t)e^{\frac{i}{2\sqrt{2}}\Theta_c^*(x,t)}B^\dagger(0,0)e^{-\frac{i}{2\sqrt{2}}\Theta_c^*(0,0)}\rangle. \tag{F13}$$

This is readily calculated using the unitary transformation (77). In the new basis the correlator factorises

$$\begin{aligned} H(x,t) &\sim \langle e^{\frac{i}{2\sqrt{2}}(\Delta N_c - N_c^{\rm imp})\Theta_c^\circ(x,t)}e^{-\frac{i}{2\sqrt{2}}(\Delta N_c - N_c^{\rm imp})\Theta_c^\circ(0,0)}\rangle\langle \widetilde{B}(x,t)\widetilde{B}^\dagger(0,0)\rangle \\ &\sim \frac{1}{(x^2 - v_c^2t^2)^\eta}\int_{-\Lambda}^{\Lambda}\frac{{\rm d}p}{2\pi}e^{-ipx}e^{-i\varepsilon(p)t}, \end{aligned} \tag{F14}$$

where in this case $\varepsilon(p)$ is given by $\varepsilon_c(\pi + p)$ and

$$\eta = \frac{1}{2K_c}\left(\frac{3}{2} + \frac{N_c^{\rm imp}}{2}\right)^2. \tag{F15}$$

Fourier transforming and using (19) we arrive at

$$\sigma_1^{(2)}(\omega)\Big|_{ph} \sim \frac{1}{\omega}\int_{-\Lambda}^{\Lambda}{\rm d}p\,\widetilde{G}^c_{\eta,\eta}\big(\omega - \varepsilon(p), p\big)\ , \tag{F16}$$

where $\widetilde{G}^c_{\eta,\eta}(\omega,p)$ is given by (104). The behaviour of (F16) is shown in Fig. 17. We see that the contribution vanishes

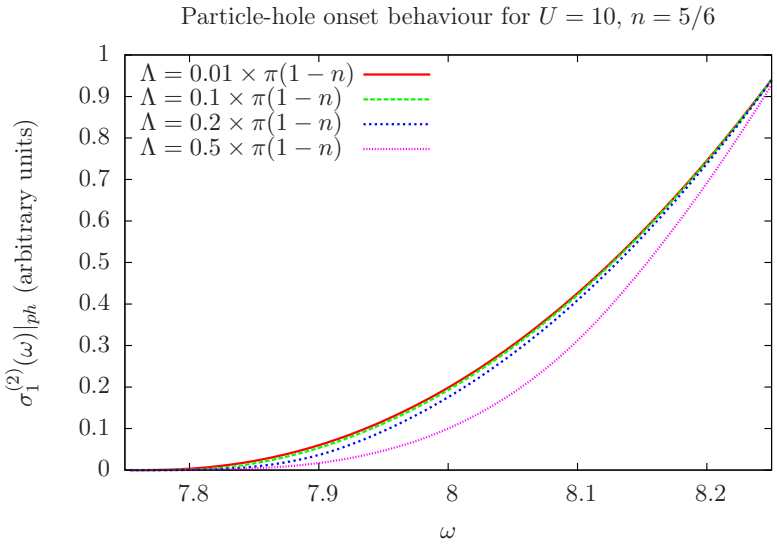


Figure 17: Contribution to onset of $\sigma_1^{(2)}(\omega)$ from particle-hole excitation in (F16) for $U = 10$, $n = 5/6$

smoothly at the threshold and increases slowly above it.

### 2. Threshold of the two-hole continuum in $\sigma_1^{(2)}(\omega)$

Last but not least we wish to consider the threshold of the contribution of the two-hole continuum to $\sigma_1^{(2)}(\omega)$. This occurs at a higher energy than the threshold of the particle-hole and particle-particle continua, but unlike the latter two persists as we approach half-filling. The threshold is parametrised by

$$E^{\rm hh}_{\rm thres}(q) = -2\varepsilon_c\left(\frac{k(q)}{2}\right) - 2\mu, \tag{F17}$$

where $k(q)$ is again fixed by (F1). The threshold corresponds to having *two* high-energy hole excitations with momentum $q/2$ each. As we are now dealing with two impurities with equal momenta, the appropriate mobile impurity model is of the form (61), but we now have to retain impurity-impurity interactions

$$H_{\rm imp} = \int {\rm d}x \left[ B^\dagger(x)(\varepsilon - iu\partial_x - \frac{1}{2m}\partial_x^2)B(x) + V\ B^\dagger(x)\partial_x B^\dagger(x)\ B(x)\partial_x B(x) \right]. \tag{F18}$$

### a. *Projection of the operator $\mathcal{O}_j$*

Next we require the projection of the operator $\mathcal{O}_j$ onto the mobile impurity model. This proceeds as before, cf. eqns (F2), (F3), but now we take

$$R_c(x) \sim r_c(x) + B^\dagger(x) e^{-iqx/2}. \tag{F19}$$

Substituting this into the expression (F3) for $\mathcal{O}(x)$ we find

$$\mathcal{O}(x) \sim e^{i(2k_F - \pi - q)x} B^\dagger(x)\partial_x B^\dagger(x) e^{\frac{i}{2\sqrt{2}}\Phi_c^*(x)} + \dots\ , \tag{F20}$$

where we have retained only the most relevant term in the sector with two impurities.

### b. *Finite-size corrections to excitation energies in the mobile impurity model*

The interactions between the mobile impurities and the Luttinger liquid degrees of freedom can again be removed by the unitary transformation (77). In the transformed basis finite-size corrections to the excitation energies in the LL part of the theory can then be calculated as before, and lead to the result (82).

The zero mode eigenvalues for the "minimal" excitation (cf. (83)) associated with $\mathcal{O}(x)$ as defined in (F20) are

$$q_c^{(0)} = -\pi\sqrt{2}\ , \quad \bar{q}_c^{(0)} = \pi\sqrt{2}\ , \quad q_s^{(0)} = 0\ , \quad \bar{q}_s^{(0)} = 0. \tag{F21}$$

### c. *Finite-size corrections to excitation energies from the Bethe Ansatz*

The two-hole excitation has been constructed in III C 3, and the threshold of interest here occurs when, in the thermodynamic limit, the two holes have equal momentum. The finite-size corrections to the excitation energy can be calculated following Ref. 25, details are given in Appendix D. The final result in zero magnetic field is

$$\begin{aligned} E = e_{GS}L - \varepsilon_c(k^{h_1}) - \varepsilon_c(k^{h_2}) - \frac{\delta k^{h_1}}{L}\varepsilon_c'(k^{h_1}) - \frac{\delta k^{h_2}}{L}\varepsilon_c'(k^{h_2}) - \frac{\pi}{6L}(v_c + v_s) \\ + \frac{2\pi v_c}{L}\left[ \frac{(\Delta N_c - N_c^{\rm imp})^2}{8K_c} + 2K_c\left( D_c - D_c^{\rm imp} + \frac{D_s - D_s^{\rm imp}}{2} \right)^2 \right] \\ + \frac{2\pi v_s}{L}\left[ \frac{1}{2}\left( \Delta N_s - N_s^{\rm imp} - \frac{\Delta N_c - N_c^{\rm imp}}{2} \right)^2 + \frac{(D_s - D_s^{\rm imp})^2}{2} \right]. \end{aligned} \tag{F22}$$

Here the ground state energy per site $e_{GS}$ and dressed energy $\varepsilon_c(k)$ are given in (35) and (36) respectively, while the velocities $v_{s,c}$ and the Luttinger parameter $K_c$ are calculated in Appendix A. The thermodynamic values $k^{h_i}$ of the impurity rapidities and the finite-size corrections $\delta k^{h_i}$ are determined by (D6) and (D7). Finally, we have

$$\begin{aligned} &\Delta N_c = 0\ , \qquad \Delta N_s = -1\ , \qquad D_c = \frac{1}{2}\ , \qquad D_s = 0\ , \\ &N_c^{\rm imp} = 2(N_s^{\rm imp} + 1) = \int_{-Q}^{Q} {\rm d}k\, \rho_{c,1}(k)\ , \qquad D_s^{\rm imp} = 0, \end{aligned} \tag{F23}$$

$$\begin{aligned} 2D_c^{\rm imp} = &\int_Q^\pi {\rm d}k\, [\rho_{c,1}(-k) - \rho_{c,1}(k)] - \sum_{j=1,2}\frac{i}{\pi}\left\{ \ln\left[ \frac{\Gamma\left(\frac{1}{2} - i\frac{\sin k^{h_j}}{4u}\right)\Gamma\left(1 + i\frac{\sin k^{h_j}}{4u}\right)}{\Gamma\left(\frac{1}{2} + i\frac{\sin k^{h_j}}{4u}\right)\Gamma\left(1 - i\frac{\sin k^{h_j}}{4u}\right)} \right] \right\} \\ &+ \frac{i}{\pi}\int_{-Q}^{Q} {\rm d}k\, \rho_{c,1}(k)\left\{ \ln\left[ \frac{\Gamma\left(\frac{1}{2} - i\frac{\sin k}{4u}\right)\Gamma\left(1 + i\frac{\sin k}{4u}\right)}{\Gamma\left(\frac{1}{2} + i\frac{\sin k}{4u}\right)\Gamma\left(1 - i\frac{\sin k}{4u}\right)} \right] \right\}, \end{aligned} \tag{F24}$$

where $\rho_{c,1}(k)$ is the solution of the integral equation

$$\rho_{c,1}(k) = -\cos k\ \left[R(\sin k - \sin k^{h_1}) + R(\sin k - \sin k^{h_2})\right] + \cos k \int_{-Q}^{Q} dk'\ \rho_{c,1}(k') R(\sin k - \sin k'). \tag{F25}$$

### *d. Fixing the parameters $\gamma_\alpha$, $\bar{\gamma}_\alpha$*

By comparing the finite-size spectra calculated from the Bethe Ansatz (F22) with those obtained from the mobile impurity model (82) we are again able to determine the parameters $\gamma_\alpha$, $\bar{\gamma}_\alpha$. In the case at hand we obtain

$$\gamma_c + \bar{\gamma}_c = -\sqrt{2} D_c^{\rm imp}\ , \quad \gamma_c - \bar{\gamma}_c = -\frac{1}{\sqrt{2}} N_c^{\rm imp}\ , \quad \gamma_s = \bar{\gamma}_s = 0. \tag{F26}$$

### *e. Current-current correlator in the mobile impurity model*

Given the expression (F20) for the projection of the operator $\mathcal{O}_j$, we have

$$\begin{aligned} C^{(2)}_{\rm JJ}(\ell, t) &\sim \langle \mathcal{O}^\dagger(x,t)\mathcal{O}(0,0)\rangle \\ &\sim \langle \partial_x B(x,t) B(x,t) e^{-i\Phi_c^*(x,t)/2\sqrt{2}} B^\dagger(0,0)\partial_x B^\dagger(0,0) e^{i\Phi_c^*(0,0)/2\sqrt{2}}\rangle \equiv L(x,t). \end{aligned} \tag{F27}$$

This is readily calculated using the unitary transformation (77). In the new basis the correlator factorises

$$\begin{aligned} L(x,t) = \langle \partial_x \widetilde{B}(x,t)\widetilde{B}(x,t)\widetilde{B}^\dagger(0,0)\partial_x\widetilde{B}^\dagger(0,0)\rangle \\ \times \big\langle e^{-i\frac{\frac{1}{2}-2D_c^{\rm imp}}{\sqrt{2}}\Phi_c^\circ(x,t) + i\frac{N_c^{\rm imp}}{\sqrt{2}}\Theta_c^\circ(x,t)} e^{i\frac{\frac{1}{2}-2D_c^{\rm imp}}{\sqrt{2}}\Phi_c^\circ(0,0) - i\frac{N_c^{\rm imp}}{\sqrt{2}}\Theta_c^\circ(0,0)}\big\rangle. \end{aligned} \tag{F28}$$

The Luttinger liquid part of the correlator is readily calculated

$$L(x,t) = \langle \partial_x \widetilde{B}(x,t)\widetilde{B}(x,t)\widetilde{B}^\dagger(0,0)\partial_x\widetilde{B}^\dagger(0,0)\rangle \big(x - v_c t\big)^{-\nu_+} \big(x + v_c t\big)^{-\nu_-}, \tag{F29}$$

where

$$\begin{aligned} \nu_\pm &= 2\left[\sqrt{K_c}\left(\frac{1}{2} - 2D_c^{\rm imp}\right) \mp \frac{N_c^{\rm imp}}{2\sqrt{K_c}}\right]^2, \\ \nu &= \nu_+ + \nu_- = 4K_c\left(\frac{1}{2} - 2D_c^{\rm imp}\right)^2 + \frac{\big(N_c^{\rm imp}\big)^2}{K_c}. \end{aligned} \tag{F30}$$

In the absence of interactions between our two high-energy impurities ($V = 0$) the impurity part of the correlator is readily calculated as

$$\langle \partial_x \widetilde{B}(x,t)\widetilde{B}(x,t)\widetilde{B}^\dagger(0,0)\partial_x\widetilde{B}^\dagger(0,0)\rangle \sim \frac{1}{t^{3/2}}\delta(x - ut). \tag{F31}$$

In order to gain some insight in the importance of interactions, they can be taken into account in a random phase approximation in the impurity-impurity interaction. Summing up the RPA bubble diagrams does not change the behaviour sufficiently close to the threshold. Putting everything together we find

$$L(x,t) \sim \frac{1}{(x - v_c t)^{\nu_+}} \frac{1}{(x + v_c t)^{\nu_-}} \frac{\delta(x - ut)}{t^{3/2}} + \dots \tag{F32}$$

The resulting contribution to $\sigma_1^{(2)}(\omega)$ for frequencies close to $\omega_0 = -2\mu - 2\varepsilon_c\left(\frac{k(q))}{2}\right)$ is thus

$$\sigma_1^{(2)}(\omega)\Big|_{\rm two-hole} \sim \frac{1}{\omega}\left(\omega - \omega_0\right)^{\nu + \frac{1}{2}}\ \Theta(\omega - \omega_0). \tag{F33}$$

As we have pointed out before, the excitation with two high-energy holes persists at half-filling. Importantly, this contribution is no longer suppressed at half-filling, and in fact gives rise to the square root increase above the absolute

threshold in the optical conductivity in this limit[28,40,41]. Our result (F33) is reconciled with this behaviour by noting that the frequency range $\omega - \omega_0$ over which (F33) holds is related to the cutoff $\Lambda_c$ of the charge sector of the Luttinger liquid degrees of freedom. As we approach half-filling this cutoff tends to zero i.e. the frequency window in which (F33) applies vanishes. At sufficiently high frequencies $\omega > \omega_0 + \Lambda_c$ we expect on general grounds to recover the square root behaviour observed at half-filling.

---


[1] J.-P. Farges, *Organic Conductors*, Marcel Dekker, New York (1994).
[2] F. H. L. Essler, H. Frahm, F. Göhmann, A. Klümper, and V. E. Korepin, *The One-Dimensional Hubbard Model*, Cambridge University Press, Cambridge (2005).
[3] F. Woynarovich, J. Phys. A **22**, 4243 (1989).
[4] H. Frahm and V. E. Korepin, Phys. Rev. B **42** 10553 (1990).
[5] F. D. M. Haldane, J. Phys. C: Solid State Phys. **14** 2585 (1981).
[6] F. D. M. Haldane, Phys. Lett. A **81**, pp. 153-155 (1981).
[7] A. O. Gogolin, A. A. Nersesyan, and A. M. Tsvelik, *Bosonization and strongly correlated systems*, Cambridge University Press (2004).
[8] T. Giamarchi, *Quantum physics in one dimension*, Clarendon Press, Oxford (2004).
[9] A. Rozhkov, Eur. Phys. J. B **47**, 193 (2005).
[10] M. Pustilnik, M. Khodas, A. Kamenev, and L. I. Glazman, Phys. Rev. Lett. **96**, 196405 (2006).
[11] A. V. Rozhkov, Phys. Rev. B **74**, 245123 (2006).
[12] E. Bettelheim, A. G. Abanov, and P. Wiegmann, Phys. Rev. Lett. **97**, 246401 (2006).
[13] R. G. Pereira, J. Sirker, J.-S. Caux, R. Hagemans, J. M. Maillet, S. R. White, and I. Affleck, Phys. Rev. Lett. **96**, 257202 (2006).
[14] M. Khodas, M. Pustilnik, A. Kamenev, and L. I. Glazman, Phys. Rev. Lett. **99**, 110405 (2007).
[15] M. Khodas, M. Pustilnik, A. Kamenev, and L. I. Glazman, Phys. Rev. B **76**, 155402 (2007).
[16] A. Imambekov and L.I. Glazman, Phys. Rev. Lett. **100**, 206805 (2008).
[17] R. G. Pereira, S. R. White, and I. Affleck, Phys. Rev. Lett. **100**, 027206 (2008).
[18] E. Bettelheim, A. G. Abanov, and P. Wiegmann, J. Phys. A**41**, 392003 (2008).
[19] V. V. Cheianov and M. Pustilnik, Phys. Rev. Lett. **100**, 126403 (2008).
[20] R. G. Pereira, S. R. White, and I. Affleck, Phys. Rev. B **79**, 165113 (2009).
[21] A. Imambekov and L. I. Glazman, Phys. Rev. Lett. **102**, 126405 (2009).
[22] A. G. Abanov, E. Bettelheim, and P. Wiegmann, J. Phys. A42, 135201 (2009).
[23] R. G. Pereira and E. Sela, Phys. Rev. B **82**, 115324 (2010).
[24] A. Imambekov and L. I. Glazman, Science **323**, 228 (2009).
[25] F. H. L. Essler, Phys. Rev. B **81**, 205120 (2010).
[26] T. L. Schmidt, A. Imambekov, and L. I. Glazman, Phys. Rev. Lett. **104**, 116403 (2010).
[27] T. L. Schmidt, A. Imambekov, and L. I. Glazman, Phys. Rev. B **82** 245104 (2010).
[28] R. G. Pereira, K. Penc, S. R. White, P. D. Sacramento, and J. M. P. Carmelo, Phys. Rev. B **85**, 165132 (2012).
[29] L. Seabra, F. H. L. Essler, F. Pollmann, I. Schneider, and T. Veness, Phys. Rev. B **90**, 245127 (2014).
[30] A. V. Rozhkov, Phys. Rev. Lett. **112**, 106403 (2014).
[31] T. Price and A. Lamacraft, Phys. Rev. B**90**, 241415 (2014).
[32] J. M. P. Carmelo, K. Penc, L. M. Martelo, P. D. Sacramento, J. M. B. Lopes Dos Santos, R. Claessen, M. Sing, and U. Schwingenschlögl, Europhys. Lett. 67, 233 (2004).
[33] J. M. P. Carmelo, K. Penc, P. D. Sacramento, M. Sing, and R. Claessen, J. Phys.: Condens. Matter 18, 5191 (2006).
[34] J. M. P. Carmelo, D. Bozi, and K. Penc, J. Phys. Cond. Mat. 20, 415103 (2008).
[35] F. H. L. Essler, R. G. Pereira, and I. Schneider, Phys. Rev. B **91**, 245150 (2015).
[36] A. Imambekov, T. L. Schmidt, and L. I. Glazman, Rev. Mod. Phys **84**, 1253 (2012).
[37] In such a case, the difference between $\varepsilon(q)$ and $\tilde{\varepsilon}(q)$ is simply a constant shift of $\sum_\alpha \pi v_\alpha \left( \frac{(\gamma_\alpha - \bar{\gamma}_\alpha)^2}{2K_\alpha} + 2K_\alpha \left(\gamma_\alpha + \bar{\gamma}_\alpha\right)^2 \right)$.
[38] R. G. Pereira, Int. J. Mod. Phys. B **26**, 1244008 (2012).
[39] L. Balents, Phys. Rev. B **61**, 4429 (2000).
[40] E. Jeckelmann, F. Gebhard, and F. H. L. Essler, Phys. Rev. Lett. **85**, 3910 (2000).
[41] D. Controzzi, F. H. L. Essler, and A. M. Tsvelik, Phys. Rev. Lett. **86**, 680 (2001).
[42] D. Controzzi, F. H. L. Essler, and A. M. Tsvelik, arXiv:cond-mat/0011439.
[43] E. Jeckelmann, Phys. Rev. B **66**, 045114 (2002).
[44] E. Jeckelmann, Phys. Rev. B **67**, 075106 (2003).
[45] H. J. Schulz, Phys. Rev. Lett. **64**, 2831 (1990).
[46] B. S. Shastry and B. Sutherland, Phys. Rev. Lett **65** 243 (1990).
[47] T. Giamarchi, Phys. Rev. B **44**, 2905 (1991).
[48] T. Giamarchi and A. J. Millis, Phys. Rev. B **46**, 9325 (1992).
[49] T. Giamarchi, Physica B: Cond. Matt. **230**, 975 (1997).

[50] J. M. P. Carmelo, N. M. R. Peres, and P. D. Sacramento, Phys. Rev. Lett. **84**, 4673 (2000).
[51] F. H. L. Essler, V. E. Korepin, K. Schoutens, Nucl. Phys. B **372**, 559 (1992).
[52] F. H. L. Essler, V. E. Korepin, K. Schoutens, Phys. Rev. Lett. **67** 3848 (1991).
F. H. L. Essler, V. E. Korepin, K. Schoutens, Nucl. Phys. B **384** 431 (1992).
[53] F. H. L. Essler and V. E. Korepin, Phys. Rev. Lett. **72**, 908 (1994).
[54] F. H. L. Essler and V. E. Korepin, Nucl. Phys. B **426**, 505 (1994).
[55] F. H. L. Essler and H. Frahm, Phys. Rev. B**60**, 8540 (1999).
[56] O. J. Heilmann, E. H. Lieb, Ann. N.Y. Acad. Sci. **172** 584 (1971)
[57] C. N. Yang, Phys. Rev. Lett. **63**, 2144 (1989).
[58] V. E. Korepin , N. M. Bogoliubov, and A. G. Izergin, *Quantum inverse scattering method and correlation functions*. Cambridge University Press, Cambridge (1997).
[59] A. C. Tiegel, T. Veness, P. E. Dargel, A. Honecker, T. Pruschke, I. P. McCulloch, and F. H. L. Essler Phys. Rev. B **93**, 125108 (2016).
[60] W. Richardson, J. Opt. Soc. Am. **62**, 55 (1972).
[61] L. B. Lucy, Astronomical J. **79**, 745 (1974).